J. Fluid Mech. (2000), *vol.* 411, *pp.* 233–262. Printed in the United Kingdom

© 2000 Cambridge University Press

Flow and reaction in solid oxide fuel cells

By R. J. COOPER, J. BILLINGHAM AND A. C. KING
School of Mathematics and Statistics, University of Birmingham, Birmingham, B15 2TT, UK

(Received 7 July 1999 and in revised form 4 November 1999)

A fuel cell is an electrochemical device that converts chemical energy into electrical energy. The essential difference between a fuel cell and a battery is that the fuel and oxidant are continually supplied to a fuel cell whereas a battery has a finite amount of fuel stored within it which eventually becomes exhausted, after which the battery has to be recharged or replaced. We consider here a tubular cell which is run on methane. A mathematical model for the reaction and transport processes in the cell is presented. This takes into account diffusion, advection and reaction as well as the electrochemical flow of oxygen. When the device is running steadily, we perform an analysis, using the method of matched asymptotic expansions to find the flow field, the mass fractions of each chemical species and the electrical power output. These results are confirmed by a numerical technique and compared with experimental results.

1. Introduction

The fundamental chemical reaction in any fuel cell is that of hydrogen with oxygen. This produces waste only in the form of water and heat, which can be used by a heat engine as a secondary source of energy. This makes the fuel cell one of the cleanest forms of energy production available and, given the need to reduce emissions of greenhouse gases, makes the development of fuel cell technology an important goal over the next few decades. Currently there is no infrastructure for large-scale hydrogen production, so instead, methane (CH_4) is used as a substitute. Methane can either react directly with oxygen (partial oxidation) or can be converted to hydrogen by a process called steam reforming. Methane is a convenient fuel to consume as it is likely to become a significant pollutant in the next century. This is due to its increased production as a consequence of the expected increase in world population and the fact that it can absorb 25 times more infra-red radiation than carbon dioxide (Blomen & Mugerwa 1993). Fuel cell systems already exist in parts of Japan and the USA, and efficiencies of over 40% have been demonstrated. This can rise to 85% if the resultant steam is used for cogeneration where the heat is also utilized. This compares with efficiencies of around 30% for existing coal-fired power stations.

Various types of fuel cell are currently under development. The electrolyte in the cell, and the mechanism by which charge is conducted in it are what sets different fuel cells apart. For example, the polymer (or proton) electrolyte membrane fuel cell (PEMFC), also known as the solid polymer fuel cell (SPFC), which can operate at relatively low temperatures (60–150°C), is being developed for use in the automobile industry. The solid oxide fuel cell (SOFC) operates at much higher temperatures, typically 600–1000°C, which allows the use of more readily-available materials such as nickel as a catalyst for the chemical reactions involved. The electrolyte is made from a ceramic solid, zirconia (ZrO_2), which has the property that at high temperatures it can conduct oxygen ions. This is often chemically stabilized by doping with yttria.

https://doi.org/10.1017/S0022112099008150 Published online by Cambridge University Press

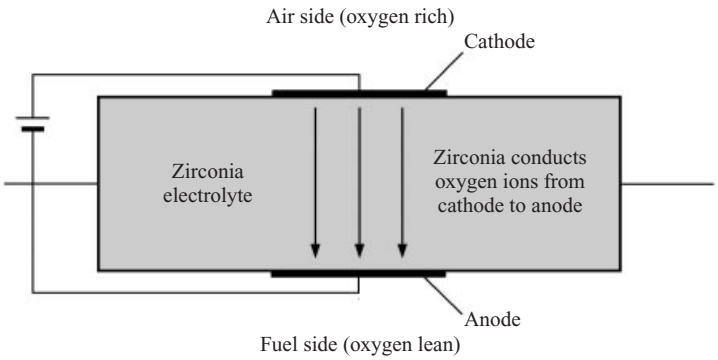


FIGURE 1. A diagram of the electrochemical principle behind the SOFC.

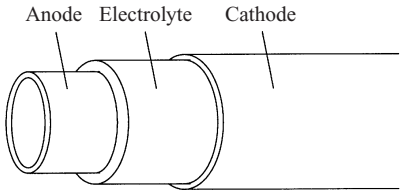


FIGURE 2. A diagram of the tubular SOFC, showing how the components fit together.

Fuel reacts with oxygen on one side of the zirconia, leaving a deficiency of oxygen molecules on that side while the other side is left exposed to the air, where the atmospheric oxygen present results in an oxygen concentration gradient across the zirconia, from high concentration on the air side to low concentration on the fuel side. An electrical connection between two electrodes placed on either side allows electrons to flow through a wire from the anode on the fuel side to the cathode on the air side, with the flow of negatively-charged oxygen ions across the zirconia in between the electrodes completing the circuit. This electrochemical principle is illustrated in figure 1. Any unburnt fuel is able to flow through the system and react with air to produce waste heat which can be utilized to form a secondary source of power, adding to the overall efficiency of the device.

There are currently two main configurations of the SOFC. The planar design consists of the zirconia electrolyte in the shape of a flat disc or square with circular electrodes on either side aligned such that the three components have a common centre. A mathematical model of the gas flow and reactions for this configuration was studied by Copcutt, King & Kendall (1996), and later refined by Billingham *et al.* (1999) to include the effect of drawing a current from the cell. The second configuration, the tubular cell, is constructed from tubes of zirconia with tubular electrodes fitted onto the inner and outer surfaces, as illustrated in figure 2. The cell we shall study (Kendall & Prica 1994), has the cathode on the outside and the anode on the inside, with a gas feed flowing into the tube. This helps to solve the problem of sealing one side from the other, although the arrangement has been successfully inverted to have the fuel on the outside (Bratton 1994). The tubes of zirconia are extruded from powders dispersed in polymer solutions to produce high thermal shock resistance and greater resistance to mechanical shocks than existing planar and tubular designs. The cathode is made from lanthanum strontium manganite and the anode is a nickel zirconia cermet. Both electrodes are pasted on to the electrolyte, made

https://doi.org/10.1017/S0022112099008150 Published online by Cambridge University Press

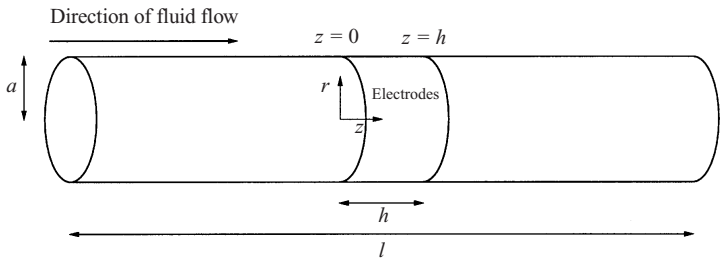


FIGURE 3. A diagram of the tubular SOFC, with the coordinate system.

from yttria-stabilized zirconia. This structure allows the integration of the electrical connections required to complete the circuit.

A diagram of the cell is shown in figure 3. The length l of the tube is 20 cm, and the internal radius a is 0.9 mm. The length h of the electrodes is 1.3 cm. The thickness of the zirconia electrolyte layer is of the order 10^{-6} m. An input mixture of methane and steam is fed into the tube at a flow rate of 25 ml min^{-1} at room temperature and immediately heated to the operating temperature of 1123 K. The molar fraction of methane is 5 times that of water in the input gas. (When the exhaust gases are sampled by a mass spectrometer a buffer of inert helium is added to the input mixture to facilitate accurate measurements of the various mass fractions.) Methane is converted to hydrogen by internal steam reforming, where the reforming process takes place inside the cell with the other reactions rather than before the fuel mixture is fed into the cell. Any unburnt fuel will in practice flow through the tube and react with oxygen at the end of the tube to produce useful heat. We now assume that the following reaction scheme:

$$CH_4 + H_2O \underset{k_2}{\overset{k_1}{\rightleftharpoons}} CO + 3H_2, \tag{1.1}$$

$$CO + H_2O \underset{k_4}{\overset{k_3}{\rightleftharpoons}} CO_2 + H_2, \tag{1.2}$$

$$2H_2 + O_2 \underset{k_6}{\overset{k_5}{\rightleftharpoons}} 2H_2O, \tag{1.3}$$

$$2CO + O_2 \underset{k_8}{\overset{k_7}{\rightleftharpoons}} 2CO_2, \tag{1.4}$$

takes place on the anode surface. Reaction (1.1) is the steam reforming reaction, which produces essential hydrogen from methane for use in the fundamental reaction (1.3). The carbon monoxide produced in reforming can also be burnt with oxygen by reaction (1.4). We will also consider the water gas shift reaction (1.2) which can occur in conjunction with steam reforming. We will use reaction rate constants $k_1 - k_8$, where k_1 represents the forward steam reforming reaction, k_2 the backwards reaction, and k_3 and k_4 the forward and backward water gas shift reactions respectively and so on. These reactions only take place on the surface of the anode on the inside of the tube. This is due to the reliance on the presence of the nickel catalyst which forms part of the anode composition. Oxygen molecules on the outside of the cell combine at the cathode with electrons to form negatively charged oxygen ions. When the cell is operating at sufficiently high temperatures, these oxygen ions can flow across the zirconia electrolyte to the anode where they are converted back into molecular oxygen and electrons. The process is summed up in the electrochemical equation

$$4O^{2-} \rightleftharpoons 2O_2 + 8e^-. \tag{1.5}$$

The oxygen then reacts with the fuel via the fundamental surface reactions (1.3) and

https://doi.org/10.1017/S0022112099008150 Published online by Cambridge University Press

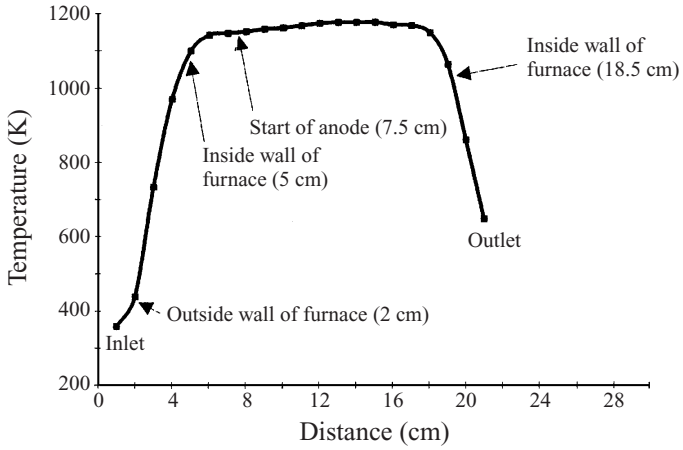


FIGURE 4. The temperature gradient along the axis of the tube. Operating temperature 1173 K, tube length = 26 cm, length of anode = 18.5 cm.

(1.4), while the electrons are carried away by the electrical circuit. An important feature of this cell, found experimentally, is that the cell temperature is spatially isothermal over the chemically active region. A typical temperature profile is shown in figure 4. Any temperature variations are small when compared with the background temperature of over 1100 K. It is clear that the cell, which is housed inside a well insulated furnace, is self-heating once the initial temperature transients have decayed and it is running under steady-state conditions.

2. A mathematical model for the cell

2.1. *A model for the electrochemical flux through the electrodes*

In the cell the current density, or flux density of electrons, $i(z)$ at any position z along the axis of the tube, is directly proportional to the flux density of oxygen molecules, $q_e(z)$, via

$$i(z) = 4Fq_e(z), \tag{2.1}$$

where F is the Faraday constant. Its typical value and those of the other physical quantities, is given in table 1. The factor 4 represents the four electrons carried by the two oxygen ions produced per oxygen molecule in the electrochemical reaction (1.5). The local electrochemical potential $E(z)$ is given by the Nernst equation (Blomen & Mugerwa 1993),

$$E(z) = \frac{RT}{4F} \ln\left(\frac{C_{oa}}{C_o(z)}\right), \tag{2.2}$$

where R is the gas constant, $C_o(z)$ is the local concentration of oxygen on the fuel side of the zirconia electrolyte, C_{oa} is the constant value of atmospheric oxygen concentration on the air side and T is the absolute temperature of the cell. The cell potential E_{cell} is related to the Nernst potential by

$$E_{cell} = E(z) - i(z)R_s. \tag{2.3}$$

R_s is the specific resistance of the zirconia, defined as the product of the resistivity and the electrolyte thickness. This equation is derived from Kirchhoff's laws by considering

https://doi.org/10.1017/S0022112099008150 Published online by Cambridge University Press

Physical quantity	Symbol	Typical value
Internal radius of the tube	a	0.9 mm
Length of the anode	h	1.3 cm
Mass flow rate of the input gas	Q_{in}	0.0875×10^{-6} kg s^{-1}
Input gas density	ρ_{in}	0.0561 kg m^{-3}
Atmospheric density	ρ_a	0.326 kg m^{-3}
Faraday's constant	F	9.6×10^{4} coulomb mol^{-1}
Gas constant	R	8.3 J K^{-1} mol^{-1}
Temperature	T	1123 K
Cell voltage	E_{cell}	0.4–1 V
Specific resistance of zirconia	R_s	$1.707\times10^{-4}\ \Omega$ m^2
Mass fraction of oxygen in the atmosphere	Y_{oa}	0.2325
Molar mass of each chemical species	m_i	$m_f = 0.016$ kg mol^{-1} $m_w = 0.018$ kg mol^{-1} $m_h = 0.002$ kg mol^{-1} $m_m = 0.028$ kg mol^{-1} $m_d = 0.044$ kg mol^{-1} $m_o = 0.032$ kg mol^{-1}
Gas diffusivity	D	10^{-4} m^2 s^{-1}
Viscosity	μ	5×10^{-5} kg m^{-1} s^{-1}

TABLE 1. Physical quantities, their symbols and typical values.

the cell as many small elements, each of which can be thought of as a local battery with its own resistance. The resistivity will in practice include the resistive effect of the electrodes. We will be able to obtain a value for R_s by fitting to experimental data. Combining (2.1), (2.2) and (2.3) we are able to obtain an expression for the flux density of oxygen ions through the zirconia in terms of the oxygen concentration and various parameters:

$$q_e(z) = \frac{RT}{16F^2R_s}\left(\ln\left(\frac{C_{oa}}{C_o(z)}\right) - \frac{4F}{RT}E_{cell}\right)\mathrm{H}(z), \tag{2.4}$$

where $\mathrm{H}(z) = H(z) - H(z-h)$ is a composite Heaviside function that appears because the electrochemical reaction is confined to the region under the electrodes ($0 \leqslant z \leqslant h$). By integrating (2.3) over the area of the electrodes we can obtain an expression for the overall current I, where $I = \int_{\theta=0}^{2\pi}\int_{z=0}^{h} a\, i(z)\,\mathrm{d}z\,\mathrm{d}\theta$, and after using equation (2.2) we obtain

$$IR_I = \frac{RT}{4Fh}\int_0^h \ln\left(\frac{C_{oa}}{C_o}\right)\,\mathrm{d}z - E_{cell}, \tag{2.5}$$

where $R_I = R_s/2\pi ah$ is the total internal resistance of the zirconia and the electrodes. Note that this expression is similar to $E_{cell} = E - IR_I$, which corresponds to an ordinary battery, although in this case $C_o(z)$ is a nonlinear function of the current I.

2.2. *Conservation of mass and momentum*

We work with the mass fraction Y_i of each chemical species in the mixture, which is related to its concentration C_i and the mixture density ρ by

$$Y_i = \frac{m_iC_i}{\rho}, \tag{2.6}$$

https://doi.org/10.1017/S0022112099008150 Published online by Cambridge University Press

where m_i is the molecular mass of species i. We will study the six species involved in the reaction scheme, and use the following subscripts for i to denote each species: f (fuel-methane), w (water), o (oxygen), h (hydrogen), m (carbon monoxide) and d (carbon dioxide).

The expression for conservation of mass in the bulk mixture is

$$\nabla \cdot (\rho \boldsymbol{v}) = 0, \tag{2.7}$$

where $\boldsymbol{v}$ is the velocity of the gas mixture and the right-hand side is equal to 0 because there is no chemical reaction in the main flow (Buckmaster & Ludford 1982). We will assume that a steady state has been reached, so that there are no time derivatives in these equations. The equation for conservation of mass for each individual species Y_i is

$$\nabla \cdot (\rho Y_i \boldsymbol{v}) - \rho_{in} D \nabla^2 Y_i = 0, \tag{2.8}$$

where ρ_{in} is the density of the input mixture and D is the diffusivity, which we will assume is constant and equal for all species.

The equation for conservation of momentum can be written as

$$\rho(\boldsymbol{v} \cdot \nabla)\boldsymbol{v} = -\nabla p + \mu \nabla^2 \boldsymbol{v} + \tfrac{1}{3}\mu \nabla(\nabla \cdot \boldsymbol{v}), \tag{2.9}$$

where μ is the coefficient of viscosity for the mixture of gases, and p is the mixture pressure. Finally we will assume that each chemical species satisfies a gas law of the form $p_i = \rho R T Y_i / m_i$. Then Dalton's law of partial pressures gives

$$p = \rho R T \sum_i \frac{Y_i}{m_i}. \tag{2.10}$$

These equations are to be solved in the cylindrical coordinate system shown in figure 3. We will assume that the solution is axisymmetric, so that the fluid velocity has only radial and axial components.

2.3. *Boundary conditions*

The input gas is composed of methane and water only. Hence the conditions at the inlet of the tube are

$$Y_f = Y_{f(in)},\ Y_w = Y_{w(in)},\ Y_h = Y_m = Y_d = Y_o = 0 \quad \text{at } z = (h-l)/2 \ \text{ for } 0 \leqslant r \leqslant a, \tag{2.11}$$

where $Y_{f(in)}$ and $Y_{w(in)}$ represent the input mass fractions of methane and water, and $Y_{f(in)} + Y_{w(in)} = 1$. Along the axis of the tube we have no flux of any species and no radial velocity so that

$$\frac{\partial Y_i}{\partial r} = 0 \quad \text{at } r = 0 \ \text{ for } (h-l)/2 \leqslant z \leqslant (h+l)/2. \tag{2.12}$$

We also have a set of mass-flux boundary conditions that model the reaction and transport processes taking place at the surface of the anode. At this surface the amount of each species that is created or consumed by chemical reaction must be balanced by the amount transported by diffusion and radial advection. The mass-flux boundary conditions are therefore

$$\rho_{in} D \frac{\partial Y_f}{\partial r} - \rho Y_f v_r = \left(-\frac{k_1 \rho^2 Y_f Y_w}{m_w} + \frac{k_2 \rho^4 Y_h^3 Y_m m_f}{m_h^3 m_m} \right) \mathrm{H}(z), \tag{2.13}$$

https://doi.org/10.1017/S0022112099008150 Published online by Cambridge University Press

$$\rho_{in}D\frac{\partial Y_w}{\partial r}-\rho Y_w v_r=\left(-\frac{k_1\rho^2 Y_f Y_w}{m_f}+\frac{k_2\rho^4 Y_h^3 Y_m m_w}{m_h^3 m_m}-\frac{k_3\rho^2 Y_m Y_w}{m_m}+\frac{k_4\rho^2 Y_d Y_h m_w}{m_d m_h}+\frac{2k_5\rho^3 Y_h^2 Y_o m_w}{m_h^2 m_o}-\frac{2k_6\rho^2 Y_w^2}{m_w}\right)\mathrm{H}(z), \quad (2.14)$$

$$\rho_{in}D\frac{\partial Y_h}{\partial r}-\rho Y_h v_r=\left(\frac{3k_1\rho^2 Y_f Y_w m_h}{m_f m_w}-\frac{3k_2\rho^4 Y_h^3 Y_m}{m_h^2 m_m}+\frac{k_3\rho^2 Y_m Y_w m_h}{m_m m_w}-\frac{k_4\rho^2 Y_d Y_h}{m_d}-\frac{2k_5\rho^3 Y_h^2 Y_o}{m_h m_o}+\frac{2k_6\rho^2 Y_w^2 m_h}{m_w^2}\right)\mathrm{H}(z), \quad (2.15)$$

$$\rho_{in}D\frac{\partial Y_m}{\partial r}-\rho Y_m v_r=\left(\frac{k_1\rho^2 Y_f Y_w m_m}{m_f m_w}-\frac{k_2\rho^4 Y_h^3 Y_m}{m_h^3}-\frac{k_3\rho^2 Y_m Y_w}{m_w}+\frac{k_4\rho^2 Y_d Y_h m_m}{m_d m_h}-\frac{2k_7\rho^3 Y_m^2 Y_o}{m_m m_o}+\frac{2k_8\rho^2 Y_d^2 m_m}{m_d^2}\right)\mathrm{H}(z), \quad (2.16)$$

$$\rho_{in}D\frac{\partial Y_d}{\partial r}-\rho Y_d v_r=\left(\frac{k_3\rho^2 Y_m Y_w m_d}{m_m m_w}-\frac{k_4\rho^2 Y_d Y_h}{m_h}+\frac{2k_7\rho^3 Y_m^2 Y_o m_d}{m_m^2 m_o}-\frac{2k_8\rho^2 Y_d^2}{m_d}\right)\mathrm{H}(z), \quad (2.17)$$

$$\rho_{in}D\frac{\partial Y_o}{\partial r}-\rho Y_o v_r=\left(m_o q_e(z)-\frac{k_5\rho^3 Y_h^2 Y_o}{m_h^2}+\frac{k_6\rho^2 Y_w^2 m_o}{m_w^2}-\frac{k_7\rho^3 Y_m^2 Y_o}{m_m^2}+\frac{k_8\rho^2 Y_d^2 m_o}{m_d^2}\right)\mathrm{H}(z), \quad (2.18)$$

where we have used the law of mass action to represent the rates of reaction. By adding together these equations, noting that $\sum_i Y_i = 1$ and hence $\sum_i \partial Y_i/\partial r = 0$, we find that

$$-\rho v_r = m_o q_e(z) \text{ at } r = a, \quad (2.19)$$

and we can substitute this back into the left-hand side of the mass-flux boundary conditions. We also have a condition for the inflow at the beginning of the tube, $z = (h-l)/2$,

$$Q_{in} = \int_{\theta=0}^{2\pi}\int_{r=0}^{a} \rho_{in} v_z r \, \mathrm{d}r \, \mathrm{d}\theta, \quad (2.20)$$

where Q_{in} is the rate of mass flux at the inlet of the tube. In addition, we have the no-slip condition in the axial direction for the fluid at the anode surface, as well as the no radial flux condition at the central axis of the tube given by

$$v_z = 0 \quad \text{at } r = a \quad \text{for } (h-l)/2 \leqslant z \leqslant (h+l)/2, \quad (2.21)$$

$$v_r = 0 \quad \text{at } r = 0 \quad \text{for } (h-l)/2 \leqslant z \leqslant (h+l)/2. \quad (2.22)$$

2.4. *Non-dimensionalization*

We begin the non-dimensionalization of the equations for conservation of mass and momentum by choosing scales based on the dimensions of the tube and other physical

https://doi.org/10.1017/S0022112099008150 Published online by Cambridge University Press

constants,

$$\left.\begin{aligned} \bar{z} &= \frac{z}{h}, \quad \bar{r} = \frac{r}{a}, \quad \bar{\rho} = \frac{\rho}{\rho_{in}}, \quad \bar{v}_z = \frac{v_z \rho_{in} \pi a^2}{Q_{in}}, \\ \bar{v}_r &= \frac{v_r \rho_{in} \pi a h}{Q_{in}}, \quad \bar{m}_i = \frac{m_i}{m_f}, \quad \bar{p} = \frac{\pi \rho_{in} a^4 (p - p_{in})}{h \mu Q_{in}}. \end{aligned}\right\} \tag{2.23}$$

Note that our scaling of the axial distance with the electrode length h, which is small compared with the length of the whole cell, allows us to treat the cell as an infinitely-long tube described by the domain $0 \leqslant \bar{r} \leqslant 1$ and $-\infty < \bar{z} < \infty$ at leading order. The electrode region is then defined by $0 \leqslant \bar{z} \leqslant 1$. The conservation-of-mass equation for the whole mixture (2.7), assuming a steady axisymmetric flow, becomes

$$\frac{1}{r}\frac{\partial}{\partial r}(r \rho v_r) + \frac{\partial}{\partial z}(\rho v_z) = 0, \tag{2.24}$$

and the conservation-of-mass equation for each individual species (2.8) becomes

$$Q\left(\frac{1}{\bar{r}}\frac{\partial}{\partial \bar{r}}(\bar{r}\bar{\rho} Y_i \bar{v}_r) + \frac{\partial}{\partial \bar{z}}(\bar{\rho} Y_i \bar{v}_z)\right) - \frac{1}{\bar{r}}\frac{\partial}{\partial \bar{r}}\left(\bar{r}\frac{\partial Y_i}{\partial \bar{r}}\right) - \epsilon^2 \frac{\partial^2 Y_i}{\partial \bar{z}^2} = 0. \tag{2.25}$$

The dimensionless equations for conservation of momentum are

$$\bar{\rho}\epsilon^2 Re\left(\bar{v}_z \frac{\partial \bar{v}_r}{\partial \bar{z}} + \bar{v}_r \frac{\partial \bar{v}_r}{\partial \bar{r}}\right) = -\frac{1}{\epsilon}\frac{\partial \bar{p}}{\partial \bar{r}} + \frac{\epsilon}{3}\left(\frac{4}{\bar{r}}\frac{\partial \bar{v}_r}{\partial \bar{r}} + 4\frac{\partial^2 \bar{v}_r}{\partial \bar{r}^2} - \frac{4}{\bar{r}^2}\bar{v}_r + \frac{\partial^2 \bar{v}_z}{\partial \bar{r}\partial \bar{z}} + 3\epsilon^2 \frac{\partial^2 \bar{v}_r}{\partial \bar{z}^2}\right), \tag{2.26}$$

$$\bar{\rho}\epsilon Re\left(\bar{v}_z \frac{\partial \bar{v}_z}{\partial \bar{z}} + \bar{v}_r \frac{\partial \bar{v}_z}{\partial \bar{r}}\right) = -\frac{\partial \bar{p}}{\partial \bar{z}} + \tfrac{1}{3}\epsilon^2\left(4\frac{\partial^2 \bar{v}_z}{\partial \bar{z}^2} + \frac{\partial^2 \bar{v}_r}{\partial \bar{r}\partial \bar{z}} + \frac{1}{\bar{r}}\frac{\partial \bar{v}_r}{\partial \bar{z}}\right) + \frac{1}{\bar{r}}\frac{\partial \bar{v}_z}{\partial \bar{r}} + \frac{\partial^2 \bar{v}_z}{\partial \bar{r}^2}, \tag{2.27}$$

and the dimensionless pressure, from (2.10), satisfies

$$\bar{p} = \frac{\gamma - 1}{\gamma P}\left(\bar{\rho}\sum_i \frac{Y_i}{\bar{m}_i} - \sum_i \frac{Y_{i(in)}}{\bar{m}_i}\right). \tag{2.28}$$

The dimensionless constants that appear in these and the remaining equations are defined in table 2, along with their typical values. The dimensionless form of the boundary conditions (2.11) and (2.12) is

$$Y_f \to Y_{f(in)}, \quad Y_w \to Y_{w(in)}, \quad Y_h, Y_m, Y_d, Y_o \to 0 \quad \text{as } \bar{z} \to -\infty \quad \text{for } 0 \leqslant \bar{r} \leqslant 1, \tag{2.29}$$

$$\frac{\partial Y_i}{\partial \bar{r}} = 0 \quad \text{at } \bar{r} = 0 \quad \text{for} \quad -\infty < \bar{z} < \infty. \tag{2.30}$$

The dimensionless mass-flux boundary conditions at $\bar{r} = 1$ are

$$\delta\left(\frac{\partial Y_f}{\partial \bar{r}} + Y_f \bar{q}_e E\right) = \epsilon^2\left(-\frac{\bar{\rho}^2 Y_f Y_w}{\bar{m}_w} + \frac{\bar{k}_2 \bar{\rho}^4 \rho_{in}^2 Y_h^3 Y_m}{\bar{m}_h^3 \bar{m}_m m_f^2}\right)\mathrm{H}(z), \tag{2.31}$$

$$\begin{aligned} \delta\left(\frac{\partial Y_w}{\partial \bar{r}} + Y_w \bar{q}_e E\right) = \epsilon^2\Bigg(&-\bar{\rho}^2 Y_f Y_w + \frac{\bar{k}_2 \bar{\rho}^4 \rho_{in}^2 Y_h^3 Y_m \bar{m}_w}{\bar{m}_h^3 \bar{m}_m m_f^2} - \frac{\bar{k}_3 \bar{\rho}^2 Y_m Y_w}{\bar{m}_m} \\ &+ \frac{\bar{k}_4 \bar{\rho}^2 Y_d Y_h \bar{m}_w}{\bar{m}_d \bar{m}_h} + \frac{2\bar{k}_5 \bar{\rho}^3 \rho_{in} Y_h^2 Y_o \bar{m}_w}{\bar{m}_h^2 \bar{m}_o m_f} - \frac{2\bar{k}_6 \bar{\rho}^2 Y_w^2}{\bar{m}_w}\Bigg)\mathrm{H}(z), \end{aligned} \tag{2.32}$$

https://doi.org/10.1017/S0022112099008150 Published online by Cambridge University Press

$$\delta\left(\frac{\partial Y_h}{\partial \bar{r}} + Y_h \bar{q}_e E\right) = \epsilon^2\left(\frac{3\bar{\rho}^2 Y_f Y_w \bar{m}_h}{\bar{m}_w} - \frac{3\bar{k}_2\bar{\rho}^4\rho_{in}^2 Y_h^3 Y_m}{\bar{m}_h^2\bar{m}_m m_f^2} + \frac{\bar{k}_3\bar{\rho}^2 Y_m Y_w \bar{m}_h}{\bar{m}_m\bar{m}_w} - \frac{\bar{k}_4\bar{\rho}^2 Y_d Y_h}{\bar{m}_d} - \frac{2\bar{k}_5\bar{\rho}^3\rho_{in} Y_h^2 Y_o}{\bar{m}_h\bar{m}_o m_f} + \frac{2\bar{k}_6\bar{\rho}^2 Y_w^2\bar{m}_h}{\bar{m}_w^2}\right)\mathrm{H}(z), \quad (2.33)$$

$$\delta\left(\frac{\partial Y_m}{\partial \bar{r}} + Y_m \bar{q}_e E\right) = \epsilon^2\left(\frac{\bar{\rho}^2 Y_f Y_w \bar{m}_m}{\bar{m}_w} - \frac{\bar{k}_2\bar{\rho}^4\rho_{in}^2 Y_h^3 Y_m}{\bar{m}_h^3 m_f^2} - \frac{\bar{k}_3\bar{\rho}^2 Y_m Y_w}{\bar{m}_w} + \frac{\bar{k}_4\bar{\rho}^2 Y_d Y_h\bar{m}_m}{\bar{m}_d\bar{m}_h} - \frac{2\bar{k}_7\bar{\rho}^3\rho_{in} Y_m^2 Y_o}{\bar{m}_m\bar{m}_o m_f} + \frac{2\bar{k}_8\bar{\rho}^2 Y_d^2\bar{m}_m}{\bar{m}_d^2}\right)\mathrm{H}(z), \quad (2.34)$$

$$\delta\left(\frac{\partial Y_d}{\partial \bar{r}} + Y_d \bar{q}_e E\right) = \epsilon^2\left(\frac{\bar{k}_3\bar{\rho}^2 Y_m Y_w \bar{m}_d}{\bar{m}_m\bar{m}_w} - \frac{\bar{k}_4\bar{\rho}^2 Y_d Y_h}{\bar{m}_h} + \frac{2\bar{k}_7\bar{\rho}^3\rho_{in} Y_m^2 Y_o\bar{m}_d}{\bar{m}_m^2\bar{m}_o m_f} - \frac{2\bar{k}_8\bar{\rho}^2 Y_d^2}{\bar{m}_d}\right)\mathrm{H}(z), \quad (2.35)$$

$$\delta\left(\frac{\partial Y_o}{\partial \bar{r}} + (Y_o - 1)\bar{q}_e E\right) = \epsilon^2\left(-\frac{\bar{k}_5\bar{\rho}^3\rho_{in} Y_h^2 Y_o}{\bar{m}_h^2 m_f} + \frac{\bar{k}_6\bar{\rho}^2 Y_w^2\bar{m}_o}{\bar{m}_w^2} - \frac{\bar{k}_7\bar{\rho}^3\rho_{in} Y_m^2 Y_o}{\bar{m}_m^2 m_f} + \frac{\bar{k}_8\bar{\rho}^2 Y_d^2\bar{m}_o}{\bar{m}_d^2}\right)\mathrm{H}(z), \quad (2.36)$$

where $\bar{q}_e = -(\sigma + \ln(\bar{\rho}Y_o))\mathrm{H}(\bar{z})$ and $\bar{k}_i = k_i/k_1$. The dimensionless parameter δ is defined as $\delta = aDm_f/k_1h^2\rho_{in}$. This parameter is small as the steam reforming reaction rate constant k_1 is large (at least $\approx 10^{12}\,\mathrm{m^4\,s^{-1}\,mol^{-1}}$) and so we can expect a situation similar to an earlier study (Rubinstein, Sternberg & Keller 1989) where reaction dominates over diffusion. The sum of the mass-flux boundary conditions (2.19) becomes

$$\bar{\rho}\bar{v}_r = -\frac{Eq_e}{Q} \quad \text{at } \bar{r} = 1 \quad \text{for } -\infty < \bar{z} < \infty, \quad (2.37)$$

and the inflow condition (2.20) becomes

$$\int_0^1 \bar{r}\bar{v}_z \,\mathrm{d}\bar{r} \to \tfrac{1}{2} \quad \text{as } \bar{z} \to -\infty \quad \text{for } 0 \leqslant \bar{r} \leqslant 1. \quad (2.38)$$

Finally, the no-slip and no-radial-flux conditions for the mixture velocity (2.21), (2.22) are expressed in dimensionless form as

$$\bar{v}_z = 0 \text{ at } \bar{r} = 1 \quad \text{for } -\infty < \bar{z} < \infty \quad (2.39)$$

$$\bar{v}_r = 0 \text{ at } \bar{r} = 0 \quad \text{for } -\infty < \bar{z} < \infty. \quad (2.40)$$

For convenience, in the rest of this paper we will omit the overbar from dimensionless variables and constants.

2.5. *Solution of the conservation of momentum equations for* $\epsilon \ll 1$

We will now make use of the small dimensionless parameter ϵ, whose size reflects the fact that the flow takes place in a long, slender tube. The equations for conservation

https://doi.org/10.1017/S0022112099008150 Published online by Cambridge University Press

Symbol	Definition	Typical value	Description
ϵ	$\dfrac{a}{h}$	0.06923	aspect ratio
σ	$\dfrac{4F}{RT}E_{cell} - \ln\left(\dfrac{\rho_a Y_{oa}}{\rho_{in}}\right)$	16.2–40.9	$\dfrac{\text{cell potential}}{\text{electrochemical potential}}$
Q	$\dfrac{Q_{in}}{\pi h \rho_{in} D}$	0.382	$\dfrac{\text{fuel flowrate}}{\text{rate of diffusion}}$
E	$\dfrac{a m_o R T}{16F^2 R_s \rho_{in} D}$	1.90×10^{-3}	$\dfrac{\text{electrochemical flux of oxygen}}{\text{diffusive flux of oxygen}}$
δ	$\dfrac{aDm_f}{k_1 h^2 \rho_{in}}$	$O(10^{-23})$–$O(10^{-17})$	$\dfrac{\text{rate of diffusion}}{\text{rate of reaction}}$
Re	$\dfrac{Q_{in}}{a\mu\pi}$	0.6187	Reynolds number $= \dfrac{\text{inertial forces}}{\text{viscous forces}}$
$\bar{m}_i$	$\dfrac{m_i}{m_f}$	$m_o = 2$	$\dfrac{\text{molar mass}}{\text{molar mass of methane}}$
γ	$c_p \Big/ \left(c_p - \dfrac{R}{m_f}\right)$	1.1	ratio of specific heats
P	$\dfrac{\mu Q_{in} h}{a^4 \pi \rho_{in}^2 T c_p}$	0.1369×10^{-5}	$\dfrac{\text{compressive energy}}{\text{thermal energy}}$

TABLE 2. Definitions and typical values of the dimensionless parameters.

of momentum, (2.26) and (2.27), show that at leading order as $\epsilon \to 0$

$$\frac{\partial p}{\partial r} = 0, \quad \frac{\partial p}{\partial z} = \frac{1}{r}\frac{\partial v_z}{\partial r} + \frac{\partial^2 v_z}{\partial r^2}. \tag{2.41}$$

These equations are to be solved subject to the boundary conditions (2.37)–(2.40). This lubrication approximation, along with the conservation-of-mass equation,

$$\frac{1}{r}\frac{\partial}{\partial r}(r\rho v_r) + \frac{\partial}{\partial z}(\rho v_z) = 0, \tag{2.42}$$

can be directly integrated to give

$$p = p(z), \tag{2.43}$$

$$v_z = \frac{E}{Q}\left(r^2 - 1\right)\frac{\left(\displaystyle\int_0^z q_e(s)\,\mathrm{d}s + \frac{Q}{2E}\right)}{\displaystyle\int_0^1 \left(s^3 - s\right)\rho(s,z)\,\mathrm{d}s}, \tag{2.44}$$

$$v_r = -\frac{E}{Q\rho r}\frac{\partial}{\partial z}\left(\frac{\left(\displaystyle\int_0^z q_e(s)\,\mathrm{d}s + \frac{Q}{2E}\right)\left(\displaystyle\int_0^r \left(s^3 - s\right)\rho(s,z)\,\mathrm{d}s\right)}{\displaystyle\int_0^1 \left(s^3 - s\right)\rho(s,z)\,\mathrm{d}s}\right). \tag{2.45}$$

We will now introduce the notation $M_R = \int_0^R \left(s^3 - s\right)\rho(s,z)\,\mathrm{d}s$, in order to simplify future expressions. This quantity is related to the axial mass flux between $r = 0$ and R. The velocity components can be substituted into the mass conservation equation

https://doi.org/10.1017/S0022112099008150 Published online by Cambridge University Press

for each species (2.25). After re-arrangement we obtain,

$$-\frac{1}{r}\frac{\partial}{\partial r}\left(r\frac{\partial Y_i}{\partial r}\right)+\frac{1}{2}Q_0\epsilon\left[(r^2-1)\frac{\partial}{\partial z}\left(\frac{\rho Y_i}{M_1}\right)-\frac{1}{r}\frac{\partial}{\partial r}\left(Y_i\frac{\partial}{\partial z}\left(\frac{M_r}{M_1}\right)\right)\right]$$
$$+\epsilon^2\left(E_0\left[(r^2-1)\frac{\partial}{\partial z}\left(\frac{\rho Y_i}{M_1}\int_0^z q_e(s)\,\mathrm{d}s\right)\right.\right.$$
$$\left.\left.-\frac{1}{r}\frac{\partial}{\partial r}\left(Y_i\frac{\partial}{\partial z}\left(\frac{M_r}{M_1}\int_0^z q_e(s)\,\mathrm{d}s\right)\right)\right]-\frac{\partial^2 Y_i}{\partial z^2}\right)=0. \tag{2.46}$$

Here we have used experimental data, which suggest that $Q = O(\epsilon)$ and $E = O(\epsilon^2)$. Hence we make the substitutions $Q = Q_0\epsilon$, $E = E_0\epsilon^2$ where Q_0 and E_0 are $O(1)$.

3. Asymptotic solution for $\delta \ll 1$, $\epsilon \ll 1$

We will now proceed to solve the mass continuity equation (2.46) for the boundary conditions (2.29)–(2.36). We will express each mass fraction in terms of a perturbation series in ϵ and δ of the form

$$Y_i = Y_{i0} + \epsilon Y_{i1} + \epsilon^2 Y_{i2} + \cdots + \frac{\delta}{\epsilon^2}\bar{Y}_{i0} + \frac{\delta}{\epsilon}\bar{Y}_{i1} + O(\delta). \tag{3.1}$$

We will soon see that the magnitudes of ϵ and δ allow us to use this form of expansion, and that it is necessary to consider the terms up to $O(\delta)$. In a similar fashion we also expand the quantities ρ, M_r and M_1 as perturbation series. P is another small parameter, reflecting the fact that the thermal energy stored in the mixture of gases is far greater than the compressive energy. For typical values of the various quantities involved $P = O(\epsilon^5)$. For $P \ll 1$ we have at leading order an expression for ρ in terms of the mass fractions, given by the dimensionless pressure equation (2.28),

$$\rho = \sum_i \frac{Y_{i(in)}}{m_i} \Big/ \sum_i \frac{Y_i}{m_i}. \tag{3.2}$$

It is now our aim to solve the dimensionless boundary value problem and find values for the mass fractions downstream of the anode. We should then be able to make predictions about the current drawn for different values of the voltage. Since δ is extremely small we can expect an asymptotic approach to be successful, and so we shall consider the double limiting process $\delta \to 0$, $\epsilon \to 0$. This is relatively straightforward as $\epsilon = O(10^{-2})$ and $\delta = O(10^{-17})$ so that $\delta = o(\epsilon^n)$ for $0 \leqslant n \leqslant 8$. As we solve the conservation-of-mass equations only up to $O(\epsilon^2)$ there will be no clash of limits.

Clearly, from the discontinuous nature of the electrochemistry and chemical reactions we should begin by considering the solution in three main regions: upstream of the anode, before any of the chemical processes have acted on the fluid; on the anode itself, where the reactions take place; and downstream of the anode, where we expect the final values of each mass fraction to emerge. We will find that we also need boundary layers at the beginning and end of the anode region. The overall asymptotic structure of the solution is shown in table 3, which also shows the orders of magnitude of the mass fractions in each region. Experimental measurements indicate that the mass fractions of methane, hydrogen and carbon monoxide are of $O(1)$ at output ($z \to \infty$), while we know that, since the input mixture is composed only of methane and water, our model must allow for a decrease in water and an increase from zero

https://doi.org/10.1017/S0022112099008150 Published online by Cambridge University Press

Upstream of anode, $z < 0$	Anode front boundary layer width $O(\epsilon)$	Anode region, $0 < z < 1$	Anode back boundary layer width $O(\epsilon)$	Downstream of anode, $z > 1$
$Y_f = Y_{f(in)}$	$Y_f = O(1)$	$Y_f = O(1)$	$Y_f = O(1)$	$Y_f = O(1)$
$Y_w = Y_{w(in)}$	$Y_w = O(1)$	$Y_w = O(\delta)$	$Y_w = O(\delta)$	$Y_w = O(\delta)$
$Y_h = 0$	$Y_h = O(1)$	$Y_h = O(1)$	$Y_h = O(1)$	$Y_h = O(1)$
$Y_m = 0$	$Y_m = O(1)$	$Y_m = O(1)$	$Y_m = O(1)$	$Y_m = O(1)$
$Y_d = 0$	$Y_d = O(\delta)$	$Y_d = O(\delta)$	$Y_d = O(\delta)$	$Y_d = O(\delta)$
$Y_o = 0$	$Y_o = O(\delta)$	$Y_o = O(\delta)$	$Y_o = O(\delta)$	$Y_o = O(\delta)$
	$z = 0$	anode	$z = 1$	

TABLE 3. The asymptotic structure of the solution.

at input to $O(1)$ at output for hydrogen and carbon monoxide. We find that the final orders of magnitude for each mass fraction are reached before the $O(1)$ anode region.

We will also neglect the reactions corresponding to rate constants k_2, k_3, k_6 and k_8. This is a valid assumption to make and has been verified experimentally. Although experimental data are scarce, we can expect the remaining four reaction rate constants to be of similar order. Hence our scaling of each constant with the steam reforming rate constant k_1 provides us with $O(1)$ quanities $\bar{k}_i$. We will use the typical values $k_1 = k_4 = k_5 = k_7 = 10^{15}\,\mathrm{m^4\,s^{-1}\,mol^{-1}}$. Next we will define a new dimensionless parameter $\bar{\sigma}$ as

$$\bar{\sigma} = -\sigma - \ln\delta \tag{3.3}$$

and we will assume that $\bar{\sigma} = O(1)$ for $\delta \ll 1$. This parameter arises when we find that the oxygen mass fraction is no larger than $O(\delta)$, i.e. $Y_o = \delta Y_{o1} + O(\delta\epsilon)$. We can think of this assumption as focusing on the range of parameters for which $\sigma = -\ln\delta + O(1)$ for $\delta \ll 1$. This makes the dimensionless flux of oxygen ions $q_{e0} = \bar{\sigma} - \ln(\rho_0 Y_{o1})$ at leading order.

3.1. *Solution in the upstream region* $z < 0$

Upstream of the anode there is no electrochemistry or chemical reaction so the mass-flux boundary conditions (2.31)–(2.36) reduce to $\partial Y_i/\partial r = 0$ at $r = 1$. There is also the condition $\partial Y_i/\partial r = 0$ at $r = 0$. The conservation-of-mass equations are also simplified and a study of the leading-order and $O(\epsilon)$ equations gives constant solutions for the leading order parts of all six mass fractions and hence the density. Therefore these constant values must be equal to the input values as $z \to -\infty$. Hence we have the simple leading-order solution

$$Y_f = Y_{f(in)}, \quad Y_w = Y_{w(in)}, \quad Y_h = Y_m = Y_d = Y_o = 0, \quad \rho = 1 \quad \text{for } z < 0, \ (0 \leqslant r \leqslant 1). \tag{3.4}$$

If we next consider the solution in the anode region given by $0 \leqslant z \leqslant 1$, where the electrochemical source of oxygen appears, an analysis of the boundary conditions leads us to the conclusion that the leading-order term in the water mass fraction Y_{w0} must be zero. Further investigation shows that all lower-order terms must also be zero until a reaction term balances with a diffusive term. This will happen at $O(\delta/\epsilon^2)$. Hence there must be a boundary layer centred at $z = 0$, in order to allow a drop

https://doi.org/10.1017/S0022112099008150 Published online by Cambridge University Press

in the order of magnitude of the water mass fraction from $O(1)$ upstream of the anode to $O(\delta/\epsilon^2)$ in the anode region. Due to the dominance of reaction processes over diffusion we can be sure that δ is far smaller than ϵ. We assume that $\delta = O(\epsilon^\mu)$, where $\mu > 8$ and expand Y_w as

$$Y_w = Y_{w0} + \epsilon Y_{w1} + \epsilon^2 Y_{w2} + \cdots + \epsilon^{\mu-3} Y_{w,\mu-3} + \frac{\delta}{\epsilon^2}\bar{Y}_{w0} + \frac{\delta}{\epsilon}\bar{Y}_{w1} + \delta\bar{Y}_{w2} + \delta\epsilon\bar{Y}_{w3} + \cdots \quad (3.5)$$

with $Y_{wj} = 0$ at $r = 1$ for $j = 0, 1, \ldots, \mu - 3$.

3.2. *Solution in the boundary layer at $z = 0$*

In this region $z = O(\epsilon)$ and we expect Y_f, Y_h and Y_m to be of $O(1)$ and $Y_w = O(\delta/\epsilon^2)$ at the downstream end of this layer. We find that the mass fractions of oxygen and carbon dioxide are small and so we write $Y_i = \delta Y_{i1} + \delta\epsilon Y_{i2} + O(\delta\epsilon^2)$ for these two species. We define a scaled boundary layer variable as $z = \epsilon\bar{z}$ where $\bar{z} = O(1)$ and in terms of this variable, the mass conservation equation (2.46) becomes

$$-\frac{1}{r}\frac{\partial}{\partial r}\left(r\frac{\partial Y_{i0}}{\partial r}\right) + \frac{Q_0}{2}\left[(r^2-1)\frac{\partial}{\partial\bar{z}}\left(\frac{\rho_0 Y_{i0}}{M_{10}}\right) - \frac{1}{r}\frac{\partial}{\partial r}\left(Y_{i0}\frac{\partial}{\partial\bar{z}}\left(\frac{M_{r0}}{M_{10}}\right)\right)\right] - \frac{\partial^2 Y_{i0}}{\partial\bar{z}^2} = 0, \quad (3.6)$$

where $M_{R0} = \int_0^R (s^3 - s)\rho_0(s, \bar{z})\,\mathrm{d}s$. This is to be solved for $-\infty < \bar{z} < \infty$, $0 \leqslant r \leqslant 1$ subject to the conditions obtained from matching with the upstream solution (3.4), $Y_{f0} \to Y_{f(in)}$, $Y_{w0} \to Y_{w(in)}$, $Y_{h0}, Y_{m0}, Y_{d0}, Y_{o0} \to 0$ as $\bar{z} \to -\infty$, and the condition $\partial Y_{i0}/\partial r = 0$ at $r = 0$. At $r = 1$, because the boundary layer is centred at the point where the electrochemistry is 'switched on', the mass–flux boundary conditions (2.31)–(2.36) reduce to no-flux conditions through the cell wall for $\bar{z} < 0$, and for $\bar{z} > 0$ we have, at leading order for the $O(1)$ mass fractions,

$$\left.\begin{aligned} \frac{\partial Y_{f0}}{\partial r} &= -\frac{\rho_0^2 Y_{f0}\bar{Y}_{w0}}{m_w}, \quad & \frac{\partial Y_{w0}}{\partial r} &= -\rho_0^2 Y_{f0}\bar{Y}_{w0}, \\ \frac{\partial Y_{h0}}{\partial r} &= \frac{3\rho_0^2 Y_{f0}\bar{Y}_{w0} m_h}{m_w}, \quad & \frac{\partial Y_{m0}}{\partial r} &= \frac{\rho_0^2 Y_{f0}\bar{Y}_{w0} m_m}{m_w}, \end{aligned}\right\} \quad (3.7)$$

and also $Y_{wj} = 0$ for $j = 0, 1, \ldots, \mu - 3$. By combining appropriate multiples of these, and taking the constant solutions for the combinations $m_w Y_{f0} - Y_{w0}$, $Y_{h0} + 3m_h Y_{f0}$ and $Y_{m0} + m_m Y_{f0}$, as given by the input conditions, we can obtain values for the major mass fractions in terms of the input values of methane and water,

$$Y_{f0} = Y_{f(in)} - \frac{Y_{w(in)}}{m_w}, \quad Y_{h0} = \frac{3m_h Y_{w(in)}}{m_w}, \quad Y_{m0} = \frac{m_m Y_{w(in)}}{m_w} \quad \text{at } r = 1. \quad (3.8)$$

The smaller mass fractions, carbon dioxide and oxygen, satisfy the equations

$$0 = -\frac{\rho_0^2 k_4 Y_{d1} Y_{h0}}{m_h} + \frac{2k_7\rho_0^3 Y_{m0}^2 Y_{o1} m_d}{m_m^2 m_o}, \quad E_0 q_{e0} = \rho_0^3 Y_{o1}\left(\frac{k_5 Y_{h0}^2}{m_h^2} + \frac{k_7 Y_{m0}^2}{m_m^2}\right), \quad (3.9)$$

which can be solved numerically. Using (3.2) we can use the expressions for the three $O(1)$ mass fractions (3.8) to give the value of ρ_0 at $r = 1$,

$$\rho_0 = \left(\frac{Y_{f(in)}}{m_f} + \frac{Y_{w(in)}}{m_w}\right) \Big/ \left(\frac{Y_{f(in)}}{m_f} + \frac{3Y_{w(in)}}{m_w}\right). \quad (3.10)$$

By matching with the anode region we find that the above boundary values for each mass fraction and the mixture density must also hold at the downstream end of

https://doi.org/10.1017/S0022112099008150 Published online by Cambridge University Press

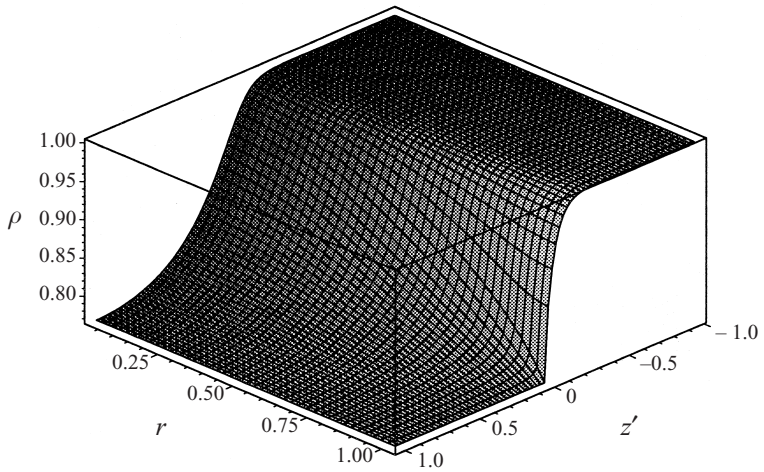


FIGURE 5. The leading-order density in the boundary layer. This was calculated using $Q_0 = 5.516$.

the boundary layer as $\bar{z} \to \infty$ for $0 \leqslant r \leqslant 1$, and hence we will in future refer to the density given by (3.10) as ρ_{out}. We now have boundary conditions for the whole of the boundary layer and a set of leading-order equations for the mass fractions (3.6). These are highly nonlinear and effectively coupled due to the appearance of the leading-order expression for the mixture density ρ_0. However we can obtain a single equation for ρ_0 by inverting both sides of (3.2) and noting that we can add appropriate multiples of (3.6) to eliminate the mass fractions:

$$-\frac{1}{r}\frac{\partial}{\partial r}\left(r\frac{\partial}{\partial r}\left(\frac{1}{\rho_0}\right)\right) + \tfrac{1}{2}Q_0\left[(r^2-1)\frac{\partial}{\partial \bar{z}}\left(\frac{1}{M_{10}}\right) - \frac{1}{r}\frac{\partial}{\partial r}\left(\frac{1}{\rho_0}\frac{\partial}{\partial \bar{z}}\left(\frac{M_{r0}}{M_{10}}\right)\right)\right] - \frac{\partial^2}{\partial \bar{z}^2}\left(\frac{1}{\rho_0}\right) = 0. \tag{3.11}$$

We will solve this numerically subject to the conditions,

$$\frac{1}{\rho_0} = \frac{1}{\rho_{out}} \text{ at } r = 1\ (\bar{z} > 0) \text{ and as } \bar{z} \to \infty\ (0 \leqslant r \leqslant 1), \tag{3.12}$$

$$\frac{1}{\rho_0} = 1 \text{ as } \bar{z} \to -\infty\ (0 \leqslant r \leqslant 1), \tag{3.13}$$

$$\frac{\partial}{\partial r}\left(\frac{1}{\rho_0}\right) = 0 \text{ at } r = 1\ (\bar{z} < 0) \text{ and } r = 0\ (-\infty < \bar{z} < \infty). \tag{3.14}$$

We will transform the infinite boundary layer domain $-\infty < \bar{z} < \infty, 0 \leqslant r \leqslant 1$ to the finite domain $0 < z' < 1, 0 \leqslant r \leqslant 1$ by use of the transformation $z' = \tanh(\bar{z}/Q_0)$, which will produce a finer grid where the solution changes most rapidly, namely close to the centre of the boundary layer. We evaluate ρ_0 at $r = r_i = ik$, $i = 0 \ldots p$, and $z' = z_j = jk$, $j = -p \ldots p$, where $p = 1/k$ and k is the stepsize. We discretize using central differences away from the boundary and using forward or backward differences as appropriate at the boundary. The integrals M_{r0} and M_{10} are evaluated using the trapezium rule. We then solve this nonlinear system using the NAG routine C05NBF which uses a combination of steepest descents and Newtonian iteration to find the solution. A typical numerically determined solution is shown in figure 5.

https://doi.org/10.1017/S0022112099008150 Published online by Cambridge University Press

Having computed a numerical solution for the leading-order density we can now proceed to use this solution in finding numerical solutions for the leading-order mass fractions. The leading-order equation for Y_{i0} is given by (3.6). Now that we have a solution for ρ_0 we can find numerical values for M_{r0} and M_{10} which allow us to solve for each Y_{i0} subject to the conditions

$$Y_{f0} \to Y_{f(in)}, \quad Y_{w0} \to Y_{w(in)}, \quad Y_{h0} \to 0, \quad Y_{m0} \to 0 \quad \text{as } \bar{z} \to -\infty, \tag{3.15}$$

$$\left.\begin{aligned} &Y_{f0} \to Y_{f(in)} - \frac{Y_{w(in)}}{m_w}, \quad Y_{w0} \to 0, \quad Y_{h0} \to \frac{3m_h Y_{w(in)}}{m_w}, \\ &Y_{m0} \to \frac{m_m Y_{w(in)}}{m_w} \quad \text{as} \quad \bar{z} \to \infty, \quad \text{and at} \quad r = 1 \quad \text{for} \quad \bar{z} > 0, \end{aligned}\right\} \tag{3.16}$$

$$\frac{\partial Y_{i0}}{\partial r} = 0 \quad \text{at} \quad r = 1 \quad \text{for} \quad \bar{z} < 0 \quad \text{and at} \quad r = 0. \tag{3.17}$$

We discretize as before, although now the integrals M_{r0} and M_{10} are known as we have a solution for ρ_0. We could attempt to solve this equation numerically using the NAG routine we used earlier. However, since the integral quantities are all known we now have a system of linear equations which can in general be expressed as a vector equation of the form $\boldsymbol{A} \cdot \boldsymbol{x} = \boldsymbol{b}$. A Gauss–Seidel iteration method, which is guaranteed to converge from any initial estimate provided the matrix $\boldsymbol{A}$ is diagonally dominant, is used to obtain numerical solutions for the mass fractions. The solutions are shown in figure 6. These illustrate how the mass fraction of water decreases from $O(1)$ and the mass fractions of hydrogen and carbon monoxide increase to $O(1)$. The mass fraction of methane decreases by a small amount due to consumption by the steam reforming reaction. We can expect similar profiles for the leading-order terms in the oxygen and carbon dioxide mass fractions, which will increase from zero at the upstream end of the boundary layer to $O(1)$ constants given by the numerically-obtained solutions to the algebraic boundary conditions (3.9), which are discussed later when the anode region is considered.

We are able to verify the numerical solutions against analytical asymptotic solutions for large $|\bar{z}|$ in the boundary layer, where the equations can be linearized. This approach leads us to an eigenvalue problem, and is described in the Appendix.

3.3. *Higher-order solutions in the boundary layer at $z = 0$*

We will now consider the solution for higher-order terms in the expansions for each mass fraction and the density. This is for the purpose of asymptotic matching with the solutions in the anode region. The $O(\epsilon)$ equations for each mass fraction in the boundary layer are given as

$$\begin{aligned} &-\frac{1}{r}\frac{\partial}{\partial r}\left(r\frac{\partial Y_{i1}}{\partial r}\right) + \frac{1}{2}Q_0\left\{\left(r^2-1\right)\frac{\partial}{\partial \bar{z}}\left[\frac{1}{M_{10}}\left(\rho_1 Y_{i0} + \rho_0 Y_{i1} - \rho_0 Y_{i0}\frac{M_{11}}{M_{10}}\right)\right]\right. \\ &\left.-\frac{1}{r}\frac{\partial}{\partial r}\left[Y_{i1}\frac{\partial}{\partial \bar{z}}\left(\frac{M_{r0}}{M_{10}}\right) + Y_{i0}\frac{\partial}{\partial \bar{z}}\left(\frac{M_{r1}}{M_{10}}\right) - Y_{i0}\frac{\partial}{\partial \bar{z}}\left(\frac{M_{r0}M_{11}}{M_{10}^2}\right)\right]\right\} - \frac{\partial^2 Y_{i1}}{\partial \bar{z}^2} = 0. \end{aligned} \tag{3.18}$$

If we consider the $O\left(\delta/\epsilon\right)$ boundary conditions at $r = 1$, we again have $\partial Y_{i1}/\partial r = 0$ for $\bar{z} < 0$. However for $\bar{z} > 0$ we have

$$\frac{\partial Y_{f1}}{\partial r} = -\frac{\rho_0^2 \bar{Y}_{w0} Y_{f0}}{m_w}\left(\frac{Y_{f1}}{Y_{f0}} + \frac{2\rho_1}{\rho_0} + \frac{\bar{Y}_{w1}}{\bar{Y}_{w0}}\right), \tag{3.19}$$

https://doi.org/10.1017/S0022112099008150 Published online by Cambridge University Press

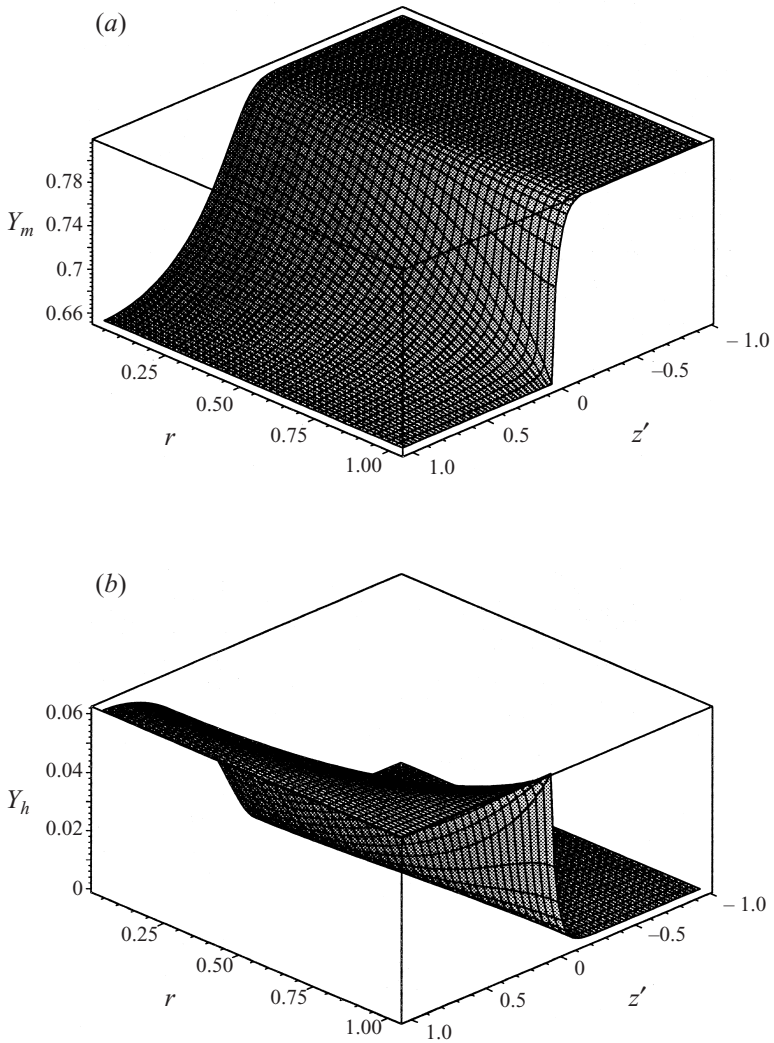


FIGURE 6 (*a*, *b*) For caption see facing page.

$$\frac{\partial Y_{w1}}{\partial r} = -\rho_0^2 \bar{Y}_{w0} Y_{f0} \left(\frac{Y_{f1}}{Y_{f0}} + \frac{2\rho_1}{\rho_0} + \frac{\bar{Y}_{w1}}{\bar{Y}_{w0}} \right), \tag{3.20}$$

$$\frac{\partial Y_{h1}}{\partial r} = \frac{3\rho_0^2 \bar{Y}_{w0} Y_{f0} m_h}{m_w} \left(\frac{Y_{f1}}{Y_{f0}} + \frac{2\rho_1}{\rho_0} + \frac{\bar{Y}_{w1}}{\bar{Y}_{w0}} \right), \tag{3.21}$$

$$\frac{\partial Y_{m1}}{\partial r} = \frac{\rho_0^2 \bar{Y}_{w0} Y_{f0} m_m}{m_w} \left(\frac{Y_{f1}}{Y_{f0}} + \frac{2\rho_1}{\rho_0} + \frac{\bar{Y}_{w1}}{\bar{Y}_{w0}} \right). \tag{3.22}$$

Adding appropriate multiples of these as earlier we again find that we can express each mass fraction in terms of the input values, which at $O(\epsilon)$ are equal to 0. Hence $Y_{f1} = Y_{m1} = Y_{h1} = Y_{w1} = 0$ at $r = 1$. These zero solutions also satisfy the main equation in the boundary layer (3.18), so we take $Y_{f1} = Y_{m1} = Y_{h1} = Y_{w1} = 0$ for $-\infty < \bar{z} < \infty$, $0 \leqslant r \leqslant 1$. We will now proceed to find asymptotic solutions for the $O(\epsilon^2)$ terms of the major mass fractions as $\bar{z} \to \infty$. These will be useful for the

https://doi.org/10.1017/S0022112099008150 Published online by Cambridge University Press

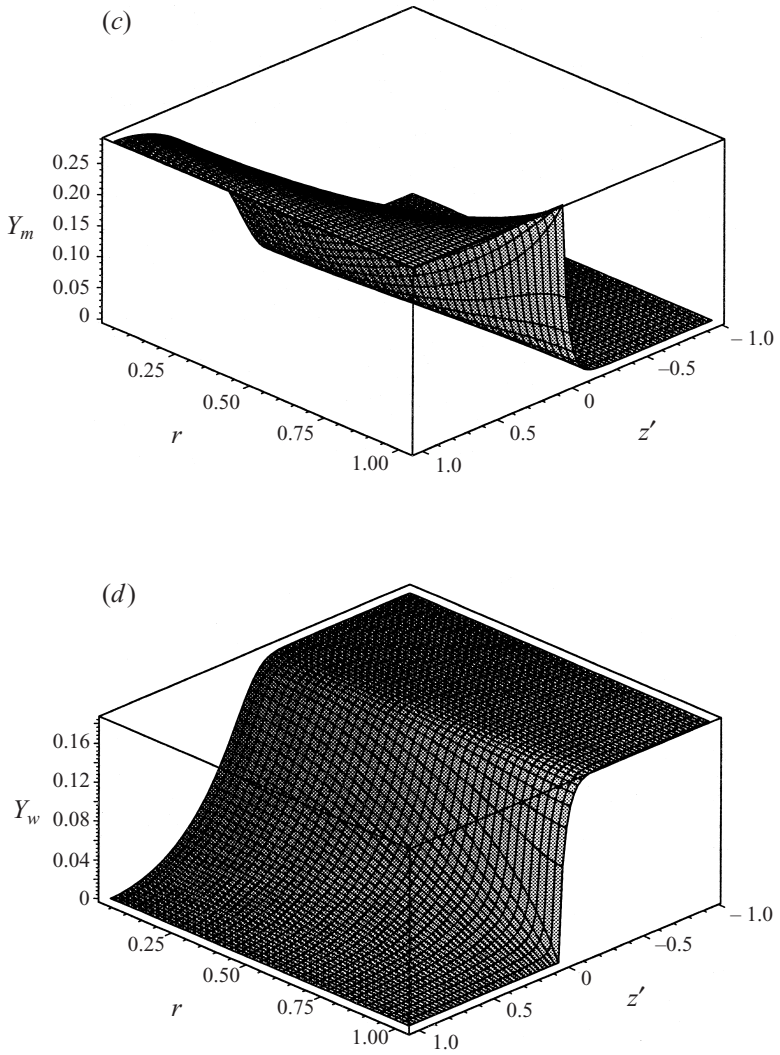


FIGURE 6. The solutions for the leading orders of four of the mass fractions in the boundary layer: (*a*) methane, (*b*) hydrogen, (*c*) carbon monoxide, (*d*) water. These were calculated using $Q_0 = 5.516$.

purpose of matching in other regions. After simplification by using the leading-order conditions for Y_o and Y_d, the mass-flux boundary condition for the $O(\epsilon^2)$ term in the water mass fraction is

$$\frac{\partial Y_{w2}}{\partial r} = \frac{2E_0 q_{e0} m_w}{m_o} - \rho_0^2 \bar{Y}_{w2} Y_{f0}, \tag{3.23}$$

where Y_{f0} is now known. We also know that Y_{w2} is zero throughout the boundary layer, so $\partial Y_{w2}/\partial r = 0$ at $r = 1$ and hence

$$\bar{Y}_{w2} = \frac{2E_0 q_{e0} m_w}{m_o \rho_0^2 Y_{f0}}. \tag{3.24}$$

This allows further simplification of the boundary conditions for the other three $O(1)$

https://doi.org/10.1017/S0022112099008150 Published online by Cambridge University Press

mass fractions:

$$\left.\begin{aligned}\frac{\partial Y_{f2}}{\partial r} &= -E_0 q_{e0}\left(Y_{f0}+\frac{2}{m_o}\right), \quad \frac{\partial Y_{h2}}{\partial r} = -E_0 q_{e0}\left(Y_{h0}-\frac{4m_h}{m_o}\right),\\ \frac{\partial Y_{m2}}{\partial r} &= -E_0 q_{e0}\left(Y_{m0}-\frac{2m_m}{m_o}\right).\end{aligned}\right\} \tag{3.25}$$

Note that the leading-order electrochemical flux, $q_{e0} = \bar{\sigma} - \ln(\rho_0 Y_{o1})$ is constant, so the right-hand side of each of these conditions is constant.

Now we consider the conservation-of-mass equation, and using the solutions for the lower orders, which enable us to simplify the expressions M_r and M_1, the equation for Y_{i2} for large $\bar{z}$ simplifies to

$$\frac{1}{r}\frac{\partial}{\partial r}\left(r\frac{\partial Y_{i2}}{\partial r}\right) + 2Q_0(r^2-1)\frac{\partial Y_{i2}}{\partial \bar{z}} + \frac{\partial^2 Y_{i2}}{\partial \bar{z}^2} = 0, \tag{3.26}$$

which is of a similar form to the equations obtained earlier for Y_{i0}. Labelling by X_i the constant values of $\partial Y_{i2}/\partial r$ at $r = 1$, as given in (3.25), we have the conditions

$$\frac{\partial Y_{i2}}{\partial r} = X_i \quad \text{at } r = 1, \qquad \frac{\partial Y_{i2}}{\partial r} = 0 \quad \text{at } r = 0, \tag{3.27}$$

and we suppose that the asymptotic behaviour of Y_{i2} for large $\bar{z}$ is of the form $Y_{i2} \sim \bar{z}^2 f_0(r) + \bar{z} f_1(r) + f_2(r)$ where f_0, f_1 and f_2 are to be determined. The boundary conditions for these functions are

$$\frac{\mathrm{d}f_2}{\mathrm{d}r} = X_i, \quad \frac{\mathrm{d}f_1}{\mathrm{d}r} = 0, \quad \frac{\mathrm{d}f_0}{\mathrm{d}r} = 0 \quad \text{at } r = 1, \tag{3.28}$$

$$\frac{\mathrm{d}f_2}{\mathrm{d}r} = 0, \quad \frac{\mathrm{d}f_1}{\mathrm{d}r} = 0, \quad \frac{\mathrm{d}f_0}{\mathrm{d}r} = 0 \quad \text{at } r = 0. \tag{3.29}$$

Substituting the suggested form into (3.26) and applying these conditions we find the solution

$$Y_{i2} \sim \frac{2X_i}{Q_0}\bar{z} + 4X_i\left(\tfrac{1}{4}r^2 - \tfrac{1}{16}r^4 + \gamma_i\right) \tag{3.30}$$

where γ_i is an unknown constant.

To summarize our work on the boundary layer at $z = 0$, the leading-order solutions for each mass fraction in the boundary layer have been found numerically, and we have verified them by using an analytical solution for large $|\bar{z}|$. For the purpose of matching with the solution in the next region we have also obtained the expressions for the main mass fractions for large $\bar{z}$,

$$\begin{aligned}Y_f \sim Y_{f(in)} - \frac{Y_{w(in)}}{m_w} + \epsilon^2\Bigg\{&\frac{-2E_0 q_{e0}}{Q_0}\left(Y_{f(in)} - \frac{Y_{w(in)}}{m_w} + \frac{2}{m_o}\right)\bar{z}\\ &-4E_0 q_{e0}\left(Y_{f(in)} - \frac{Y_{w(in)}}{m_w} + \frac{2}{m_o}\right)\left(\tfrac{1}{4}r^2 - \tfrac{1}{16}r^4 + \gamma_f\right)\Bigg\} + O(\epsilon^3),\end{aligned} \tag{3.31}$$

$$\begin{aligned}Y_h \sim \frac{3m_h Y_{w(in)}}{m_w} + \epsilon^2\Bigg\{&\frac{-2E_0 q_{e0}}{Q_0}\left(\frac{3m_h Y_{w(in)}}{m_w} - \frac{4m_h}{m_o}\right)\bar{z}\\ &-4E_0 q_{e0}\left(\frac{3m_h Y_{w(in)}}{m_w} - \frac{4m_h}{m_o}\right)\left(\tfrac{1}{4}r^2 - \tfrac{1}{16}r^4 + \gamma_h\right)\Bigg\} + O(\epsilon^3),\end{aligned} \tag{3.32}$$

https://doi.org/10.1017/S0022112099008150 Published online by Cambridge University Press

$$Y_m \sim \frac{m_m Y_{w(in)}}{m_w} + \epsilon^2 \left\{ \frac{-2E_0 q_{e0}}{Q_0} \left(\frac{m_m Y_{w(in)}}{m_w} - \frac{2m_m}{m_o} \right) \bar{z} \right.$$
$$\left. -4E_0 q_{e0} \left(\frac{m_m Y_{w(in)}}{m_w} - \frac{2m_m}{m_o} \right) \left(\tfrac{1}{4} r^2 - \tfrac{1}{16} r^4 + \gamma_m \right) \right\} + O(\epsilon^3), \quad (3.33)$$

where $q_{e0} = \bar{\sigma} - \ln(\rho_0 Y_{o1}^*)$ and Y_{o1}^* is the constant boundary value of Y_{o1}.

4. Solution in the anode region $0 \leqslant z \leqslant 1$

We can now consider the solution of the main equations in the $O(1)$ anode region. We know that the water mass fraction $Y_w = O(\delta/\epsilon^2)$, so the leading-order boundary condition for water gives $\rho_0^2 Y_{f0} \bar{Y}_{w0} = 0$ at $r = 1$. Hence $\bar{Y}_{w0} = 0$ at $r = 1$ also. Due to the presence of this factor in the other conditions we find

$$\frac{\partial Y_{f0}}{\partial r} = \frac{\partial Y_{h0}}{\partial r} = \frac{\partial Y_{m0}}{\partial r} = 0 \quad \text{at } r = 1. \quad (4.1)$$

Similarly, the second-order boundary condition for water gives

$$\rho_0^2 \bar{Y}_{w0} Y_{f0} \left(\frac{Y_{f1}}{Y_{f0}} + \frac{2\rho_1}{\rho_0} + \frac{\bar{Y}_{w1}}{\bar{Y}_{w0}} \right) = 0 \quad \text{at } r = 1, \quad (4.2)$$

and since $\bar{Y}_{w0} = 0$ at $r = 1$ this implies $\bar{Y}_{w1} = 0$ at $r = 1$ also and in turn

$$\frac{\partial Y_{f1}}{\partial r} = \frac{\partial Y_{h1}}{\partial r} = \frac{\partial Y_{m1}}{\partial r} = 0 \quad \text{at } r = 1. \quad (4.3)$$

At $O(\delta)$ we again find that the first non-zero term in the expansion for the water mass fraction on the anode boundary is

$$\bar{Y}_{w2} = \frac{2E_0 q_{e0}(z) m_w}{m_o \rho_0^2 Y_{f0}} \text{ at } r = 1, \quad (4.4)$$

and again we can make one final simplification to the other $O(\epsilon^2)$ conditions:

$$\left. \begin{aligned} \frac{\partial Y_{f2}}{\partial r} &= -E_0 q_{e0} \left(Y_{f0} + \frac{2}{m_o} \right), \quad \frac{\partial Y_{h2}}{\partial r} = -E_0 q_{e0} \left(Y_{h0} - \frac{4m_h}{m_o} \right), \\ \frac{\partial Y_{m2}}{\partial r} &= -E_0 q_{e0} \left(Y_{m0} - \frac{2m_m}{m_o} \right). \end{aligned} \right\} \quad (4.5)$$

Referring back to the main equation (2.46), at $O(\delta/\epsilon^2)$ for Y_w,

$$\frac{1}{r} \frac{\partial}{\partial r} \left(r \frac{\partial \bar{Y}_{w0}}{\partial r} \right) = 0, \quad (4.6)$$

since the two terms which precede $\bar{Y}_{w0}$ in the perturbation expansion are zero. This gives $\bar{Y}_{w0} = \bar{Y}_{w0}(z)$ and since $\bar{Y}_{w0} = 0$ at $r = 1$ we have $\bar{Y}_{w0} = 0$ for all $0 \leqslant r \leqslant 1$. Similarly at $O(\delta/\epsilon)$ we find $\bar{Y}_{w1} = 0$ and so at the next order we find $\bar{Y}_{w2} = \bar{Y}_{w2}(z)$. Therefore by (4.4) we deduce that $\bar{Y}_{w2}(z)$ must take its value at $r = 1$:

$$\bar{Y}_{w2} = \frac{2E_0 q_{e0}(z) m_w}{m_o \rho_0^2(z,1) Y_{f0}(z,1)}. \quad (4.7)$$

Now we can consider the $O(1)$ mass fractions, Y_f, Y_h and Y_m. As we found earlier, at leading order there is no radial variation and so $Y_{i0} = Y_{i0}(z)$ for $i = f, h, m$, which automatically satisfies the conditions $\partial Y_{i0}/\partial r = 0$ at $r = 0, 1$. By (3.2) we also

https://doi.org/10.1017/S0022112099008150 Published online by Cambridge University Press

have $\rho_0 = \rho_0(z)$. This can be substituted into the $O(\epsilon)$ equation for Y_{i1}, which after simplification becomes

$$-\frac{1}{r}\frac{\partial}{\partial r}\left(r\frac{\partial Y_{i1}}{\partial r}\right) + 2Q_0(1-r^2)\frac{\mathrm{d}Y_{i0}}{\mathrm{d}z} = 0. \tag{4.8}$$

We can integrate this and use the conditions that $\partial Y_{i1}/\partial r = 0$ at $r = 0$ and $r = 1$ to deduce that $\mathrm{d}Y_{i0}/\mathrm{d}z = 0$, and hence Y_{i0} and ρ_0 are constant, and $Y_{i1} = Y_{i1}(z)$, which gives us also that $\rho_1 = \rho_1(z)$. We can now simplify the expression for $\bar{Y}_{w2}$ (4.7):

$$\bar{Y}_{w2} = \frac{2E_0 q_{e0}(z) m_w}{m_o \rho_0^2 Y_{f0}}, \tag{4.9}$$

where now the only possible variable is $q_{e0}(z)$.

Now let us consider the main equation at $O(\epsilon^2)$. Making use of the properties of Y_{i0}, Y_{i1}, ρ_0 and ρ_1 already found we have

$$-\frac{1}{r}\frac{\partial}{\partial r}\left(r\frac{\partial Y_{i2}}{\partial r}\right) + 2Q_0(1-r^2)\frac{\mathrm{d}Y_{i1}}{\mathrm{d}z} = 0, \tag{4.10}$$

which is similar to the simplified equation at $O(\epsilon)$. Integrating as before and applying the symmetry condition we find

$$\frac{\partial Y_{i2}}{\partial r} = 2Q_0\left(\tfrac{1}{2}r - \tfrac{1}{4}r^3\right)\frac{\mathrm{d}Y_{i1}}{\mathrm{d}z}. \tag{4.11}$$

When we apply the boundary conditions at $r = 1$, which are given by (4.5), we obtain

$$\frac{1}{2}Q_0\frac{\mathrm{d}Y_{f1}}{\mathrm{d}z} = -E_0 q_{e0}(z)\left(Y_{f0} + \frac{2}{m_o}\right), \tag{4.12}$$

$$\frac{1}{2}Q_0\frac{\mathrm{d}Y_{h1}}{\mathrm{d}z} = -E_0 q_{e0}(z)\left(Y_{h0} - \frac{4m_h}{m_o}\right), \tag{4.13}$$

$$\frac{1}{2}Q_0\frac{\mathrm{d}Y_{m1}}{\mathrm{d}z} = -E_0 q_{e0}(z)\left(Y_{m0} - \frac{2m_m}{m_o}\right), \tag{4.14}$$

which hold at $r = 1$. However since $Y_{i1} = Y_{i1}(z)$ these must also hold for $0 \leqslant r \leqslant 1$. Integrating with respect to z,

$$Y_{f1} = -\frac{2E_0}{Q_0}\left(Y_{f0} + \frac{2}{m_o}\right)\int_0^z q_{e0}(s)\,\mathrm{d}s + c_f, \tag{4.15}$$

$$Y_{h1} = -\frac{2E_0}{Q_0}\left(Y_{h0} - \frac{4m_h}{m_o}\right)\int_0^z q_{e0}(s)\,\mathrm{d}s + c_h, \tag{4.16}$$

$$Y_{m1} = -\frac{2E_0}{Q_0}\left(Y_{m0} - \frac{2m_m}{m_o}\right)\int_0^z q_{e0}(s)\,\mathrm{d}s + c_m, \tag{4.17}$$

where c_f, c_h and c_m are constants which will be determined.

We now consider the mass fractions of oxygen and carbon dioxide, which are $O(\delta)$. At leading order, as for the other species, we find no radial variation and so we look to the boundary condition at $r = 1$. The leading-order boundary conditions for these species are

$$0 = -\frac{k_4\rho_0^2 Y_{d1} Y_{h0}}{m_h} + \frac{2k_7 m_d \rho_0^3 Y_{m0}^2 Y_{o1}}{m_m^2 m_0}, \quad E_0 q_{e0} = \rho_0^3 Y_{o1}\left(\frac{k_5 Y_{h0}^2}{m_h^2} + \frac{k_7 Y_{m0}^2}{m_m^2}\right). \tag{4.18}$$

https://doi.org/10.1017/S0022112099008150 Published online by Cambridge University Press

Note that they take the form of algebraic equations rather than differential equations. This is because these two species are not involved in the steam reforming reaction, which rules out the possibility of a leading-order balance between a diffusive term and a reactive term in the boundary conditions. Note that the oxygen condition is of the form $a - \ln(Y_{o1}) = bY_{o1}$ where a and b are constants. This is because $q_{e0} = \bar{\sigma} - \ln(\rho_0 Y_{o1})$. Since $b > 0$ we can deduce that this equation has a unique solution. Furthermore this solution, which can easily be found numerically using Newton–Raphson iteration, is independent of z, which means that Y_{o1} is constant throughout the anode region. Labelling this constant value Y_{o1}^*, we can substitute it into the carbon dioxide condition to obtain the constant solution Y_{d1}^* to the carbon dioxide mass fraction. Since the only possible axial variation in q_{e0} comes from the oxygen mass fraction, which we now know is constant at leading order, we deduce that q_{e0} is constant. Hence $\int_0^z q_{e0}(s)\,\mathrm{d}s = q_{e0}z$ and so the $O(\epsilon)$ terms for Y_f, Y_h and Y_m (4.15)–(4.17) are linear functions of z,

$$Y_{f1} = -\frac{2E_0}{Q_0}\left(Y_{f0} + \frac{2}{m_o}\right) q_{e0}z + c_f, \tag{4.19}$$

$$Y_{h1} = -\frac{2E_0}{Q_0}\left(Y_{h0} - \frac{4m_h}{m_o}\right) q_{e0}z + c_h, \tag{4.20}$$

$$Y_{m1} = -\frac{2E_0}{Q_0}\left(Y_{m0} - \frac{2m_m}{m_o}\right) q_{e0}z + c_m. \tag{4.21}$$

To summarize the solutions in the anode region,

$$Y_f = Y_{f0} + \epsilon\left(-\frac{2E_0}{Q_0}\left(Y_{f0} + \frac{2}{m_o}\right) q_{e0}z + c_f\right) + O(\epsilon^2), \tag{4.22}$$

$$Y_h = Y_{h0} + \epsilon\left(-\frac{2E_0}{Q_0}\left(Y_{h0} - \frac{4m_h}{m_o}\right) q_{e0}z + c_h\right) + O(\epsilon^2), \tag{4.23}$$

$$Y_m = Y_{m0} + \epsilon\left(-\frac{2E_0}{Q_0}\left(Y_{m0} - \frac{2m_m}{m_o}\right) q_{e0}z + c_m\right) + O(\epsilon^2), \tag{4.24}$$

$$Y_w = \delta\frac{2E_0 m_w q_{e0}}{m_o \rho_0^2 Y_{f0}} + O(\delta\epsilon), \tag{4.25}$$

$$Y_o = \delta Y_{o1}^* + O(\delta\epsilon), \tag{4.26}$$

$$Y_d = \delta Y_{d1}^* + O(\delta\epsilon). \tag{4.27}$$

In order to match the $O(\epsilon)$ terms we consider the boundary layer solutions as $\bar{z} \to \infty$. By matching the $O(1)$ terms, we find that the leading-order terms Y_{i0} are precisely the values given by the solution to the boundary conditions in the boundary layer, and by matching at $O(\epsilon)$ we obtain $c_f = c_h = c_m = 0$, and so we can complete the first two terms in the anode region solution,

$$Y_f = Y_{f(in)} - \frac{Y_{w(in)}}{m_w} - \epsilon\frac{2E_0 q_{e0}z}{Q_0}\left(Y_{f(in)} - \frac{Y_{w(in)}}{m_w} + \frac{2}{m_o}\right) + O(\epsilon^2), \tag{4.28}$$

$$Y_h = \frac{3m_h Y_{w(in)}}{m_w} - \epsilon\frac{2E_0 q_{e0}z}{Q_0}\left(\frac{3m_h Y_{w(in)}}{m_w} - \frac{4m_h}{m_o}\right) + O(\epsilon^2), \tag{4.29}$$

https://doi.org/10.1017/S0022112099008150 Published online by Cambridge University Press

$$Y_m = \frac{m_m Y_{w(in)}}{m_w} - \epsilon \frac{2E_0 q_{e0} z}{Q_0} \left(\frac{m_m Y_{w(in)}}{m_w} - \frac{2m_m}{m_o} \right) + O(\epsilon^2), \tag{4.30}$$

$$Y_w = \delta \frac{2E_0 m_w q_{e0}}{m_o \rho_0^2 \left(Y_{f(in)} - Y_{w(in)}/m_w \right)} + O(\delta\epsilon), \tag{4.31}$$

$$Y_o = \delta Y_{o1}^* + O(\delta\epsilon), \tag{4.32}$$

$$Y_d = \delta Y_{d1}^* + O(\delta\epsilon). \tag{4.33}$$

5. Solution in the downstream region $z > 1$

In this region there is no electrochemical flux of oxygen ions and no chemical reaction. The quantity $\int_0^z q_{e0}(s)\,\mathrm{d}s$ takes its final value $\int_0^1 q_{e0}(s)\,\mathrm{d}s = q_{e0} = \bar{\sigma} - \ln(\rho_0 Y_{o1})$ at leading order. This quantity is proportional to the total dimensionless current (and also the total dimensionless electrochemical flux of oxygen by (2.1)). We omit many of the details of the analysis in this region, as the equations are similar to those for the upstream region $z < 0$. As before we find that all mass fractions Y_i are constant up to exponential order. However, in order to match with the solutions in the preceding anode region, where the $O(\epsilon)$ correction has a non-zero derivative, we must introduce a boundary layer centred on $z = 1$. This boundary layer also has thickness $O(\epsilon)$. Writing $z = 1 + \epsilon\hat{z}$, we find that the leading-order boundary layer equations are exactly as for the boundary layer at $z = 0$. We have the usual conditions $\partial Y_i/\partial r = 0$ at $r = 1$ for $\hat{z} > 0$ and $r = 0$ respectively, as well as the now familiar mass-flux conditions given by (3.7) at $r = 1$ for $\hat{z} < 0$. However, from matching with the solution in the anode region we have $Y_{w0} = 0$ and hence $\partial Y_{w0}/\partial r = 0$ and in turn $\partial Y_{i0}/\partial r = 0$ at $r = 1$ for $i = f, h, m$, since each of the mass-flux conditions has the factor $\rho_0^2 Y_{f0} \bar{Y}_{w0}$. Similarly for the $O(\epsilon)$ boundary conditions, since $Y_{w1} = 0$ throughout the anode region we have $\partial Y_{w1}/\partial r = 0$ and so for this to hold at $r = 1$ we deduce that

$$-\rho_0^2 \bar{Y}_{w0} Y_{f0} \left(\frac{Y_{f1}}{Y_{f0}} + \frac{2\rho_1}{\rho_0} + \frac{\bar{Y}_{w1}}{\bar{Y}_{w0}} \right) = 0, \tag{5.1}$$

and so $\partial Y_{i1}/\partial r = 0$ at $r = 1$ for $i = f, h, m$. We take the constant solution for the first two terms in the expansions for Y_f, Y_h and Y_m. As well as satisfying the equations and all boundary conditions they also match with the (constant) downstream solutions as $\hat{z} \to \infty$. We can also match this with the anode solutions as $\hat{z} \to -\infty$. In effect this second boundary layer simply allows us to adjust the non-zero gradient at $O(\epsilon)$ to zero, in the solutions for the major three mass fractions. This gradient becomes part of the $O(\epsilon^3)$ term when we make the substitution $z = 1 + \epsilon\hat{z}$ in the anode solution. Hence the final solutions at output in the downstream region are

$$Y_f = Y_{f(in)} - \frac{Y_{w(in)}}{m_w} - \epsilon \frac{2E_0 q_{e0}}{Q_0} \left(Y_{f(in)} - \frac{Y_{w(in)}}{m_w} + \frac{2}{m_o} \right) + O(\epsilon^2), \tag{5.2}$$

$$Y_h = \frac{3m_h Y_{w(in)}}{m_w} - \epsilon \frac{2E_0 q_{e0}}{Q_0} \left(\frac{3m_h Y_{w(in)}}{m_w} - \frac{4m_h}{m_o} \right) + O(\epsilon^2), \tag{5.3}$$

$$Y_m = \frac{m_m Y_{w(in)}}{m_w} - \epsilon \frac{2E_0 q_{e0}}{Q_0} \left(\frac{m_m Y_{w(in)}}{m_w} - \frac{2m_m}{m_o} \right) + O(\epsilon^2). \tag{5.4}$$

https://doi.org/10.1017/S0022112099008150 Published online by Cambridge University Press

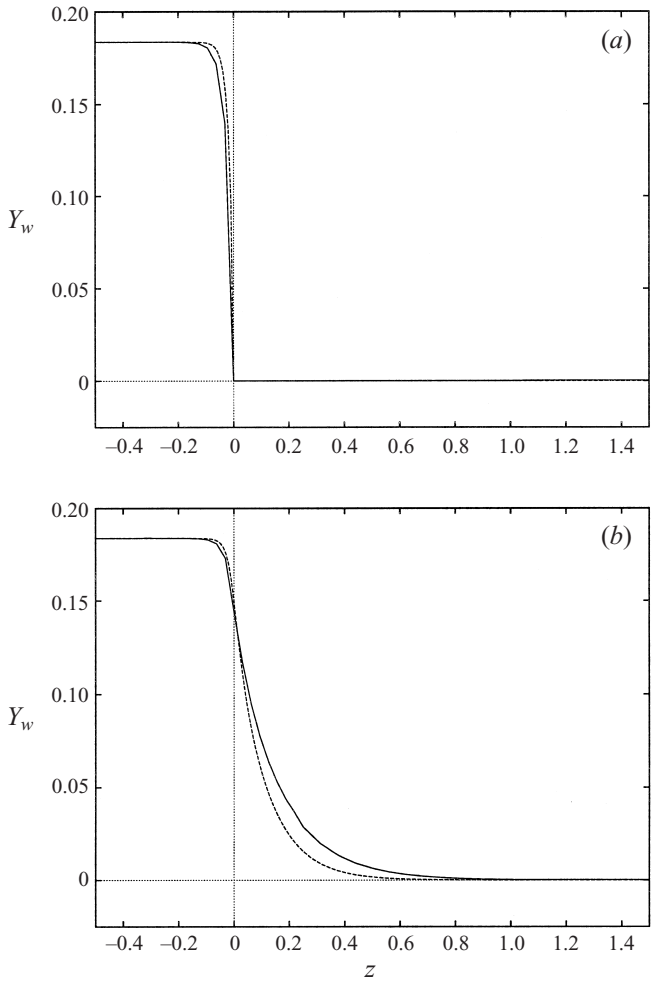


FIGURE 7. Comparison of the numerical (solid line) and analytical (dashed line) solutions for the water mass fraction Y_w: (*a*) $r = 1$, (*b*) $r = \frac{1}{2}$.

6. Numerical solution

We next consider the possibility of finding numerical solutions of the full nonlinear problem. These will be used to confirm our asymptotic analysis. The unperturbed conservation of mass equation for Y_i is given by (2.46). We will solve this numerically in the domain $0 \leqslant r \leqslant 1$, $-\frac{1}{2} \leqslant z \leqslant \frac{3}{2}$, so we in effect consider the upstream and downstream regions for half an anode length, the anode region being $0 \leqslant z \leqslant 1$. The equations are discretized by writing the independent variables as $r = r_i = ik$ ($i = 0, 1 \ldots p$) and $z = z_j = jk$ ($j = -p/2, -p/2 + 1 \ldots 3p/2$), where k is the stepsize and $p = 1/k$. As in the earlier numerical work in the boundary layer at $z = 0$, central differences are used to represent the derivatives, with forward or backward differences as appropriate at the boundary. The trapezium rule is used to represent the integral quantities. Since the mass-flux boundary conditions for each mass fraction are coupled we have to solve for all six mass fractions simultaneously, although the condition $\sum_i Y_i = 1$ allows us to consider just five. We shall use (3.2) to express the density in terms of the mass fractions. The system of five second-order partial differential

https://doi.org/10.1017/S0022112099008150 Published online by Cambridge University Press

equations is solved subject to the upstream conditions $Y_f = Y_{f(in)}, Y_w = Y_{w(in)}, Y_h = Y_m = Y_o = Y_d = 0$ at $z = -\frac{1}{2}$ and the downstream conditions $\partial Y_i/\partial z = 0$ at $z = \frac{3}{2}$. On the central axis of the tube at $r = 0$ we have $\partial Y_i/\partial r = 0$ and at $r = 1$ we have the mass-flux boundary conditions (2.31)–(2.36). The system is solved using the NAG routine C05NBF and the solutions exhibit many of the features of the analytical solutions, with a boundary layer structure at the beginning of the anode allowing the major changes in each mass fraction to take place. Two examples of the comparison between the numerical and analytical results are illustrated in figure 7. The numerical solutions used $\epsilon = 0.1$, $\sigma = 22.8$ and $R_s = 1.707 \times 10^{-4}$.

7. Comparison with experimental results

The cell, as described earlier, is housed in a custom-built furnace operated by a Eurotherm 822 controller which allows linear temperature control from room temperature up to 1373 K. Since yttria-stabilized zirconia is a good thermal insulator, the ends of the electrolyte tube which project beyond the outer walls of the furnace remain sufficiently cool for a gas-tight seal to be made with the stainless steel manifold using a silicone-rubber sealant. The cell inlet is connected to the gas manifold, which allows complete flexibility in the choice of the fuel-to-steam ratio, as well as the fuel itself. The gas stream can be instantly switched between various gas combination mixtures, enabling evaluation over a wide range of operating conditions and fuel compositions. When measurements are required we use a helium buffer to reduce the concentrations of mixture components to a level which the mass spectrometer can measure accurately. In this comparison the gas consists of 90% helium which, being inert, remains unreacted throughout the tube. The reactor outlet is linked to an on-line quadrupole mass spectrometer which allows the reactions to be directly studied. The electrical performance of the cell was measured using a custom-built potentiostat, allowing any operating potential between 0 and 1.5 V. We have experimental data on the variation of each of the mass fractions at the outlet of the cell with cell voltage, and the corresponding current variation. All results presented are for a cell temperature of 1173 K, using a methane-to-steam molar fraction ratio of 5. We can express the leading-order electrochemical flux q_{e0} as

$$q_{e0} = -\frac{4F}{RT}E_{cell} + \ln\left(\frac{\rho_a Y_{oa} h^2}{a m_f \rho_0}\right) + \ln\left(\frac{k_1}{D Y_{o1}}\right), \tag{7.1}$$

where the logarithmic term has been split into two logarithms, one of known quantities and another containing two unknown quantities k_1 and D and the oxygen mass fraction Y_{o1}. Our results have shown that Y_{o1} is independent of z and so we can integrate the dimensionless form of (2.5) easily to obtain

$$I = \frac{\pi a h R T}{2F R_s}\left(\ln\left(\frac{\rho_a Y_{oa} h^2}{\rho_0 a m_f}\right) + \ln\left(\frac{k_1}{D Y_{o1}}\right)\right) - \frac{2\pi a h}{R_s}E_{cell}. \tag{7.2}$$

We will assume that Y_{o1} varies with the cell potential via $Y_{o1} = \alpha \exp(-\beta E_{cell} + \gamma)$ where α, β and γ are unknown constants. Numerical experiments indicate that this is an acceptable assumption for positive $O(1)$ values of β. This allows us to form a linear relationship between current and cell potential, from which we can obtain expressions for the specific resistance R_s in terms of β and the combination $k_1/D\alpha$ in terms of γ by using a least-squares fit to the experimental data. This least-squares fit is shown with the corresponding experimental data in figure 8. We can now use

https://doi.org/10.1017/S0022112099008150 Published online by Cambridge University Press

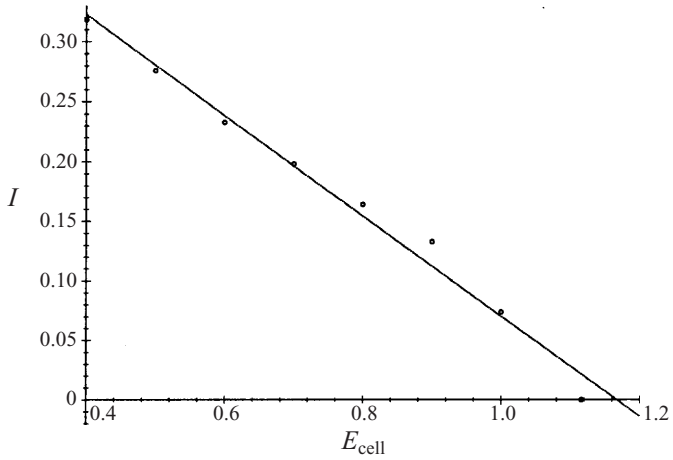


FIGURE 8. The experimentally-obtained values for the current drawn from the cell against cell voltage. The straight line of best-fit $I = 0.4905 - 0.4202E_{cell}$ is also shown.

these values to give linear expressions in E_{cell} for the output values of the $O(1)$ mass fractions,

$$Y_f = Y_{f(in)} - \frac{Y_{w(in)}}{m_w} - \epsilon\frac{2E_0}{Q_0}\left(\left(\beta - \frac{4F}{RT}\right)E_{cell} + \ln\left(\frac{\rho_a Y_{oa}h^2}{am_f\rho_0}\right) + \ln\left(\frac{k_1}{D\alpha}\right) - \gamma\right)\left(Y_{f(in)} - \frac{Y_{w(in)}}{m_w} + \frac{2}{m_o}\right), \quad (7.3)$$

$$Y_h = \frac{3m_h Y_{w(in)}}{m_w} - \epsilon\frac{2E_0}{Q_0}\left(\left(\beta - \frac{4F}{RT}\right)E_{cell} + \ln\left(\frac{\rho_a Y_{oa}h^2}{am_f\rho_0}\right) + \ln\left(\frac{k_1}{D\alpha}\right) - \gamma\right)\left(\frac{3m_h Y_{w(in)}}{m_w} - \frac{4m_h}{m_o}\right), \quad (7.4)$$

$$Y_m = \frac{m_m Y_{w(in)}}{m_w} - \epsilon\frac{2E_0}{Q_0}\left(\left(\beta - \frac{4F}{RT}\right)E_{cell} + \ln\left(\frac{\rho_a Y_{oa}h^2}{am_f\rho_0}\right) + \ln\left(\frac{k_1}{D\alpha}\right) - \gamma\right)\left(\frac{m_m Y_{w(in)}}{m_w} - \frac{2m_m}{m_o}\right). \quad (7.5)$$

These straight lines are shown in figure 9 along with the experimental data. The figures show that our model has predicted trends for the variation of the major mass fractions with the cell potential in good agreement with the experimental results. However, the predicted variation with respect to cell potential is not as large as has been observed experimentally.

8. Conclusions

Our analysis has shown that we can model the flow and reaction processes in a loaded tubular solid oxide fuel cell. Our analytical solutions are consistent with the numerical analysis and show reasonable agreement with experimental results. The

https://doi.org/10.1017/S0022112099008150 Published online by Cambridge University Press

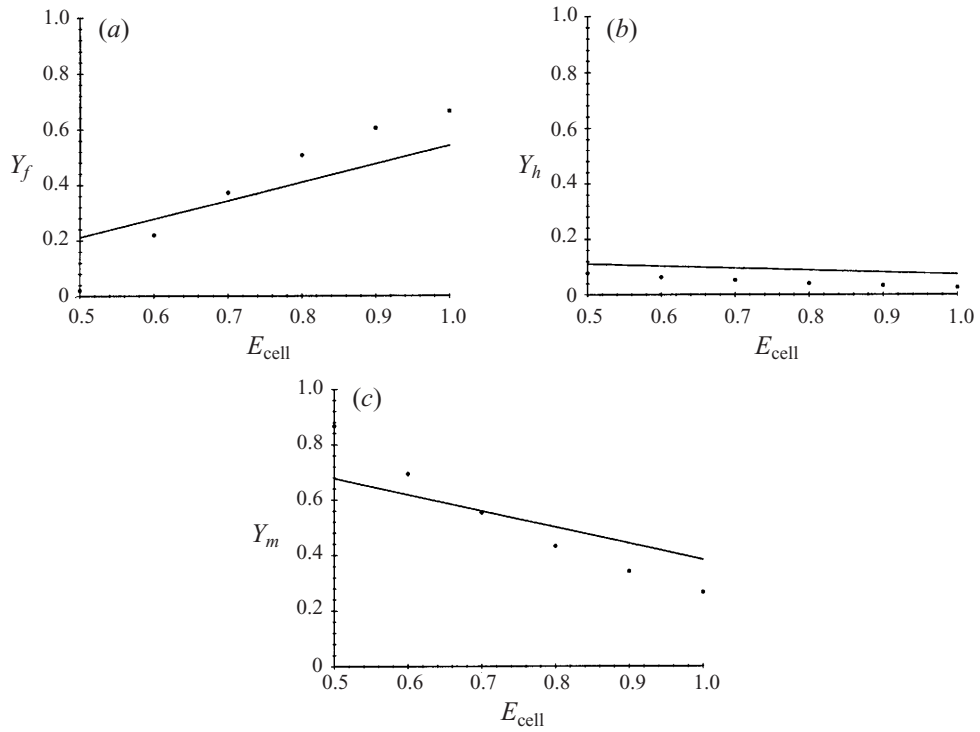


FIGURE 9. The solutions for the three $O(1)$ mass fractions as functions of cell voltage. The experimental data are represented by the dots.

next stage in our work will be to introduce several new features into the model in order to obtain better agreement with the experiments. First, it would appear that the reversibility of the water–gas shift reaction (1.2) may require consideration. The resulting extra carbon dioxide that is produced may force us to alter the assumptions made about the order of magnitude of this species. Secondly, the effects of carbon formation have so far been neglected. Carbon can form on the anode surface through various reactions, the two most important of which are

$$2\text{CO} \rightleftharpoons \text{CO}_2 + \text{C} \text{ (the Boudouard reaction)}, \tag{8.1}$$

$$\text{CH}_4 \rightleftharpoons \text{C} + 2\text{H}_2 \text{ (pyrolysis of methane)}. \tag{8.2}$$

Carbon formation via pyrolysis can block the electrodes and impair the efficiency of the cell. However, it is understood that when large currents are drawn the cell can be in effect 'self-cleaning' and remove the carbon. Our future work will involve the investigation of this effect via the introduction of reactions (8.1) and (8.2). Thirdly, we will consider the effect of one more reaction. As outlined in the introduction, methane can also be consumed by the process of partial oxidation, in which methane reacts directly with the oxygen brought in through the zirconia, as hydrogen and carbon monoxide do in our present model. We will therefore introduce the reaction

$$2\text{CH}_4 + \text{O}_2 \rightleftharpoons 2\text{CO} + 4\text{H}_2. \tag{8.3}$$

With these extra considerations, it is expected that we can obtain a more physically realistic model and achieve better agreement with the experimental results.

https://doi.org/10.1017/S0022112099008150 Published online by Cambridge University Press

This work was sponsored by the EPSRC. The authors would also like to thank Professor K. Kendall, Dr R. Cunningham and Dr C. Finnerty for providing the experimental data along with their insight into the chemistry of the tubular SOFC.

Appendix. Comparison between the numerical and analytical solutions of the anode front boundary layer equations

We expect that $\rho_0 \to 1$ as $\bar{z} \to -\infty$ and $\rho \to \rho_{out}$ as $\bar{z} \to \infty$. We can use this to simplify the nonlinear equation (3.11) and find an asymptotic solution for large $|\bar{z}|$. Moreover this can be used to check our numerical solution. Consider the behaviour of ρ_0 as $\bar{z} \to -\infty$. Writing $\rho_0 = 1 + \bar{\rho}_0$, where $\bar{\rho}_0$ is a small correction term, we can simplify M_r and M_1 to

$$M_r = \int_0^r (s^3 - s)\rho_0(s, \bar{z})\,\mathrm{d}s = \tfrac{1}{4}r^4 - \tfrac{1}{2}r^2 + \int_0^r (s^3 - s)\bar{\rho}_0(s, \bar{z})\,\mathrm{d}s, \tag{A 1}$$

$$M_1 = \int_0^1 (s^3 - s)\rho_0(s, \bar{z})\,\mathrm{d}s = -\tfrac{1}{4} + \int_0^1 (s^3 - s)\bar{\rho}_0(s, \bar{z})\,\mathrm{d}s. \tag{A 2}$$

When (A 1) and (A 2) are substituted into (3.11), we obtain the linearized equation for $\bar{\rho}_0$:

$$\frac{1}{r}\frac{\partial}{\partial r}\left(r\frac{\partial \bar{\rho}_0}{\partial r}\right) + 2Q_0\left(r^2 - 1\right)\frac{\partial \bar{\rho}_0}{\partial \bar{z}} + \frac{\partial^2 \bar{\rho}_0}{\partial \bar{z}^2} = 0. \tag{A 3}$$

The same equation arises at leading order if we consider the behaviour of ρ_0 as $\bar{z} \to \infty$ by writing $\rho_0 = \rho_{out} + \bar{\rho}_0$. Hence for large $|\bar{z}|$ we have the linear partial differential equation (A 3) and the conditions

$$\bar{\rho}_0 \to 0 \text{ as } \bar{z} \to \pm\infty \ (0 \leqslant r \leqslant 1), \tag{A 4}$$

$$\bar{\rho}_0 = 0 \text{ at } r = 1 \ (\bar{z} > 0), \tag{A 5}$$

$$\frac{\partial \bar{\rho}_0}{\partial r} = 0 \text{ at } r = 0 \ (-\infty < \bar{z} < \infty) \text{ and } r = 1 \ (\bar{z} < 0). \tag{A 6}$$

We will present the analysis for $\bar{z} \to -\infty$, although the corresponding work for $\bar{z} \to \infty$ is similar. We suppose that we can find separable solutions of the form

$$\bar{\rho}_0 = \sum_{j=0}^{\infty} a_j \mathrm{e}^{\mu_j \bar{z}} R_j^-(r) \tag{A 7}$$

where $0 < \mu_0 < \mu_1 < \mu_2 \ldots$ are eigenvalues which are to be determined. We can simplify the analysis by making the transformation $r = \lambda \bar{r}$ where $\lambda = \left(2Q_0\mu_j\right)^{-1/4}$ and for convenience writing $\alpha_j = \lambda^2\left(\mu_j^2 - 2Q_0\mu_j\right)$. When (A 7) is substituted into (A 3) we obtain

$$\frac{\mathrm{d}^2 R_j^-}{\mathrm{d}\bar{r}^2} + \frac{1}{\bar{r}}\frac{\mathrm{d}R_j^-}{\mathrm{d}\bar{r}} + \left(\alpha_j + \bar{r}^2\right)R_j^- = 0. \tag{A 8}$$

Note that the boundary conditions (A 6) become $\partial \bar{\rho}_0/\partial \bar{r} = 0$ at $\bar{r} = 0$ and $\bar{r} = 1/\lambda$. We seek to use the method of Frobenius to obtain a power series solution for R_j^-. If we write $R_j^- = \sum_{n=0}^{\infty} a_n \bar{r}^{n+c}$ we obtain a complicated three-step recurrence relation. We can avoid this by writing $R_j^- = \exp(\mathrm{i}\bar{r}^2/2)Y(\bar{r})$ which further simplifies the differential

https://doi.org/10.1017/S0022112099008150 Published online by Cambridge University Press

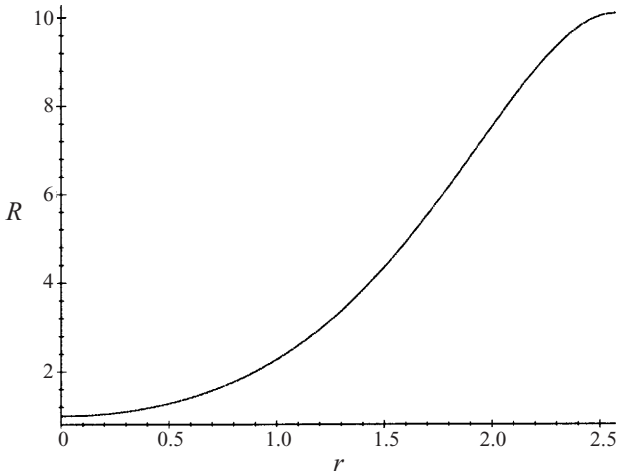


FIGURE 10. The first eigenfunction $R_0^-(\bar{r})$.

equation to

$$\frac{\mathrm{d}^2 Y}{\mathrm{d}\bar{r}^2} + \left(2\mathrm{i}\bar{r} + \frac{1}{\bar{r}}\right)\frac{\mathrm{d}Y}{\mathrm{d}\bar{r}} + \left(2\mathrm{i} + \alpha_j\right) Y = 0. \tag{A 9}$$

Now we can apply Frobenius' method using the power series expansion $Y = \sum_{n=0}^{\infty} a_n \bar{r}^{n+c}$. When this is substituted into (A 9) we find that the indicial equation is given by $a_0 c^2 = 0$ which has the double root $c = 0$. In general this implies that the second linearly independent solution has a logarithmic factor, but we can ignore this since we require a solution which is bounded as $r \to 0$. Using $c = 0$, we find that $a_{2n+1} = 0$ and

$$a_{2n} = \frac{a_0(-\frac{1}{4}i)^n \prod_{k=1}^{n}\left(\alpha_j + 2\mathrm{i}\,(2k+1)\right)}{(n!)^2} \quad \text{for } n = 0, 1, 2\ldots. \tag{A 10}$$

Hence the eigenfunction R_j^- can be written as

$$R_j^-(\bar{r}) = \exp\left(\frac{\mathrm{i}\bar{r}^2}{2}\right)\sum_{n=0}^{\infty}\frac{a_0(-\frac{1}{4}i)^n \prod_{k=1}^{n}\left(\alpha_j + 2\mathrm{i}\,(2k+1)\right)}{(n!)^2}\bar{r}^{2n}. \tag{A 11}$$

By differentiating with respect to $\bar{r}$ we see that the condition at $\bar{r} = 0$ is automatically satisfied and in order to satisfy the other condition we have an eigenvalue problem to solve for μ_j,

$$\exp\left(\frac{\mathrm{i}}{2\lambda^2}\right)\sum_{n=0}^{\infty}\left((-\tfrac{1}{4})^n\frac{a_0}{(n!)^2}\prod_{k=1}^{n}(\alpha_j + (2k-1)2\mathrm{i})\left(2n\lambda^{1-2n} + \mathrm{i}\lambda^{-1-2n}\right)\right) = 0, \tag{A 12}$$

where $\lambda = (2Q_0\mu_j)^{-1/4}$ and $\alpha_j = \lambda^2(\mu_j^2 - 2Q_0\mu_j)$. Despite the presence of the imaginary number i we find that $R_j^-(\bar{r})$ is in fact a real expression. Using MapleV we are able to show that the imaginary part is zero and, working with the real part only and taking the summation to 50 terms, we can determine the first eigenvalue as $\mu_0 = 3.960$ to 4 significant figures. The corresponding value of $1/\lambda$, which gives us the transformed position of the anode on the wall of the tube, is 2.571. The eigenfunction $R_0^-(\bar{r})$ is

https://doi.org/10.1017/S0022112099008150 Published online by Cambridge University Press

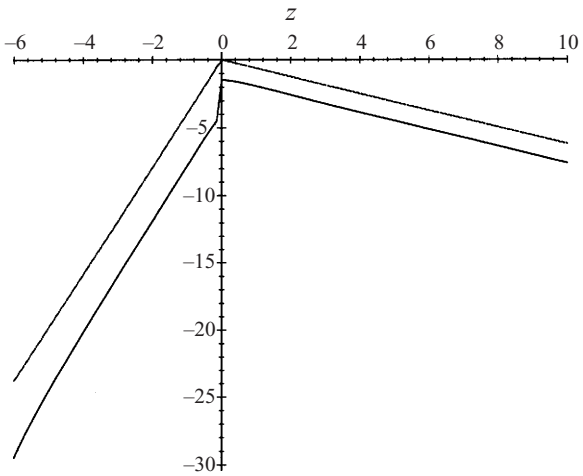


FIGURE 11. The logarithmic plot of $\ln(1-\rho_0(0,\bar{z}))$ for $\bar{z}<0$ and $\ln(\rho_0(0,\bar{z})-\rho_{out})$ for $\bar{z}>0$. We can see that this compares well with the straight lines with gradients given by the eigenvalues for the two regions.

shown in figure 10. We can proceed to find more eigenvalues, but as these will all be greater than μ_0, and our solution is asymptotically valid for large but negative $\bar{z}$, the dominance of the contribution from the first eigenvalue will be enough to render the other contributions negligible. Hence we conclude that, as $\bar{z}\to-\infty$,

$$\rho_0 \sim 1 + A_0 \exp(\mu_0\bar{z}) R_0^-(\bar{r}) + o(\exp(\mu_0\bar{z})) \tag{A 13}$$

where the constant $A_0<0$ remains undetermined. The main benefit of this analysis is that we can compare the first eigenvalue with our numerical results to gain confidence in the numerical scheme we used.

We took the numerical data we have for the leading-order density ρ_0, given in figure 5, and used the values given in the plane $r=0$, where the contribution from the eigenfunctions is always equal to 1, to create a two-dimensional plot. The z' coordinate was transformed back to the original boundary layer variable $\bar{z}$ by $\bar{z}=Q_0\tanh^{-1}(z')$ and for $\bar{z}<0$ we plotted $\ln(1-\rho_0(0,\bar{z}))$ on the vertical axis, and for $\bar{z}>0$ we plotted $\ln(\rho_0(0,\bar{z})-\rho_{out})$. By taking the natural logarithm of (A 13) we can see that this will produce straight line graphs in each half of the plane with gradients which correspond to the eigenvalues obtained in the analysis. The resulting straight line graphs are shown in figure 11. The measured gradients of these graphs are 4.0 for $\bar{z}<0$ (compared with the eigenvalue 3.960) and -0.62 for $\bar{z}>0$. Note that in this region a similar analysis to the above gave an eigenvalue $\sigma_0=0.6194$ to 4 significant figures. Hence there is agreement with the eigenvalues to 3 decimal places. The figure also shows the lines $y=\mu_0\bar{z}$ for $\bar{z}<0$ and $y=-\sigma_0\bar{z}$ for $\bar{z}>0$, which go through the origin. This shows how good the agreement is between the numerical and analytical solutions.

REFERENCES

BILLINGHAM, J., KING, A. C., COPCUTT, R. C. & KENDALL, K. 1999 Analysis of a model for a loaded, planar, solid oxide fuel cell. *SIAM J. Appl. Maths* (in press).

BLOMEN, L. J. M. J. & MUGERWA, M. N. 1993 *Fuel Cell Systems*. Plenum.

BRATTON, R. J. 1994 Westinghouse solid oxide fuel cell development program. *Proc. 1st European Solid Oxide Fuel Cell Forum* (ed. U. Bossel), pp. 887–898.

https://doi.org/10.1017/S0022112099008150 Published online by Cambridge University Press

Buckmaster, J. D. & Ludford, G. S. S. 1982 *Theory of Laminar Flames.* Cambridge University Press.

Copcutt, R. C., King, A. C. & Kendall, K. 1996 Reaction-diffusion of fuel with air between planar solid oxide fuel cells stacked with ceramic felt. *Proc. R. Soc. Lond.* A **452**, 2639–2653.

Rubinstein, J., Sternberg, P. & Keller, J. B. 1989 Fast reaction, slow diffusion and curve shortening. *SIAM J. Appl. Maths* **49**, 116–133.

https://doi.org/10.1017/S0022112099008150 Published online by Cambridge University Press